



This is the peer reviewed version of the following article:

Jayaramulu, K., Geyer, F., Schneemann, A., Kment, Š., Otyepka, M., Zboril, R., et al. (2019). Hydrophobic Metal-Organic Frameworks. *Advanced Materials*, 31(32): 1900820. doi:10.1002/adma.201900820.

, which has been published in final form at: 10.1002/adma.201900820

Hydrophobic Metal-Organic Frameworks

Jayaramulu, K., Geyer, F., Schneemann, A., Kment, Š., Otyepka, M.,
Zboril, R., et al.

This article may be used for non-commercial purposes in accordance with
publisher's Terms and Conditions for Use of Self-Archived Versions

Hydrophobic Metal-Organic Frameworks

Kolleboyina Jayaramulu,* Florian Geyer, Andreas Schneemann, Štěpán Kment, Michal Otyepka, Radek Zboril, Doris Vollmer and Roland A. Fischer*

Dr. K. Jayaramulu, Dr. A Schneemann, Prof. R. A. Fischer
Chair of Inorganic and Metal-Organic Chemistry, Department of Chemistry and Catalysis
Research Centre, Technical University of Munich, 85748 Garching, Germany
E-mail: jaya.kolleboyina@tum.de
E-mail: roland.fischer@tum.de

Dr. K. Jayaramulu, Dr. Š. Kment, Prof. M. Otyepka, Prof. R. Zboril
Regional Centre of Advanced Technologies and Materials,
Faculty of Science, Palacky University, Šlechtitelů 27, 783 71, Olomouc, Czech Republic.

Dr. F. Geyer, Prof. D. Vollmer,
Max Planck Institute for Polymer Research, Ackermannweg 10, 55128 Mainz, Germany

Dr. A Schneemann
Sandia National Laboratories, 7011 East Avenue, Livermore, CA 94551, USA

Keywords: Metal-organic Frameworks (MOFs), Hydrophobicity, Contact Angles, Hydrocarbon Separation, Oil-Water Separation.

Abstract

Metal-organic frameworks (MOFs) have diverse potential applications in catalysis, gas storage, separation, and drug delivery because of their nanoscale periodicity, permanent porosity, channel functionalization and structural diversity. Despite these promising properties, the inherent structural features of even some of the best-performing well-known MOFs make them moisture-sensitive and unstable in aqueous media, limiting their practical usefulness. This problem could be overcome by developing stable hydrophobic MOFs whose chemical composition is tuned to ensure that their metal-ligand bonds persist even in the presence of moisture and water. However, the design and fabrication of such hydrophobic MOFs poses a significant challenge. The aim of this review is to critically summarize reported syntheses of hydrophobic MOFs, highlighting issues relating to their design, characterization, and practical use. We begin with an introduction into wetting of hydrophobic materials and continue by discussing the four main strategies for synthesizing hydrophobic MOFs: (i) synthesis using organic linkers decorated with alkyl or fluorinated groups, (ii) post-synthetic modification of MOFs with hydrophobic groups, (iii) introduction of external surface corrugation using aromatic hydrocarbon building blocks, and finally (iv) the preparation of hierarchical porous hydrophobic MOF composites whose overall hydrophobicity may be due to the use of an intrinsically hydrophobic MOF or a hydrophobic two-dimensional material. Afterward, we discuss critical challenges in quantifying the wettability of these hydrophobic porous surfaces, and solutions to these challenges. Finally, we summarize the reported uses of hydrophobic MOFs in practical applications such as hydrocarbon storage/separation, and their use in separating oil spills from water. We conclude by summarizing the state of the art and highlighting some promising future developments of hydrophobic MOFs.

1 Introduction

Over the past two decades, novel hybrid nanoporous metal–organic frameworks (MOFs) have been developed as a new class of tunable hybrid materials comprised of ordered networks formed from organic ligands and metal cations.^[1-10] They are typically synthesized under mild conditions via coordination-directed self-assembly processes and are also known as metal-organic coordination networks (MCNs) and porous coordination polymers (PCPs).^[11-14] Due to their high surface areas, large porosity, tunable pore sizes, and functionalities, MOFs have prospective applications in fields such as gas storage/separation, sensing or recognition, proton conduction, and magnetism.^[14-28] However, the advantageous unique structural features of even some of the best-performing eminent MOFs are readily degraded because of their high moisture sensitivity, which may limit their practical applications.^[29-32]

Consequently, there is an ongoing search for highly hydrophobic, porous, sorbent materials to be employed in various large-scale applications in industry such as oil spill cleanup, hydrocarbon storage/separation or water purification.^[33-37] Many academics, industrial scientists, and engineers have therefore conducted research on the fabrication of superhydrophobic surfaces, which involves hydrophobic surface modification and creating surface roughness on the micrometer or nano- scale. Hydrophobic surfaces are defined as substrates with an apparent contact greater than 90° with respect to water, while surfaces of superhydrophobic materials have contact angles above 150° and very low adhesion to water droplets because drops partially rest on an air cushion. The surface energy and roughness govern the wettability of hydrophobic surfaces. In general, lower surface energies, and higher roughness are associated with larger contact angles, lower contact angle hysteresis, and robust superhydrophobicity. Because of their ultralow surface energies (10–20 mN m⁻¹), fluorinated or alkyl-based compounds are commonly used as conformal hydrophobic modifiers to prepare surfaces with high intrinsic contact angles (>90°).^[33-42] Many methods have been developed for synthesizing hydrophobic MOFs including both pristine and composite systems.^[43-99]

This review offers an overview of the state of the art in hydrophobic MOF synthesis and the field's challenges and opportunities. Various synthetic strategies for preparing hydrophobic MOFs and their composites are introduced. We discuss the basics of wetting, and critical challenges in the characterization of these hydrophobic materials. The potential applications of hydrophobic MOFs and related composites in hydrocarbon separation, water purification, and oil-spill clean-up, catalysis are then elucidated. Finally, we offer some perspectives on future directions for this promising field.

2 Wettability of (MOF) Surfaces

2.1 Describing Wettability - The Young Equation

Wettability determines the adhesion of drops to window panes, paint to cars, and ice aggregation on airplanes.^[105] Wettability is commonly tuned in printing, microfluidics,^[106] and heat transfer applications,^[107-111] and also in MOF fabrication.^[112-114] Many natural surfaces such as the wings of insects and birds are superhydrophobic what is essential to their function.^[115-116]

The degree of wetting of a drop on a surface is determined by the interfacial tension between the phases in contact, namely the liquid, solid, and gas (air). The fundamental equation correlating a droplet's macroscopic shape with its interfacial tension on an ideally flat, homogenous, solid surface was developed by Thomas Young in 1805 (Eq. 1):^[117]

$$\cos \theta = \frac{\gamma_{SG} - \gamma_{SL}}{\gamma_{LG}} \quad (1)$$

Here, γ_{SG} , γ_{SL} , and γ_{LG} are the solid-gas, solid-liquid, and liquid-gas interfacial tensions, respectively. The angle θ is called the Young or intrinsic contact angle and is measured at the three-phase contact line where the liquid, solid, and gas phases meet. The Young equation describes the balance of forces acting parallel to the solid surface at the three-phase contact line in terms of the surface tensions. It should be noted that all interfacial tensions are measured in units of force per unit length.

Surfaces with a water contact angle below 90° are considered hydrophilic, while those with water contact angles above 90° are considered to be hydrophobic.^[104, 118] Consequently, MOFs that show water contact angles above 90° are regarded as hydrophobic.

Young's equation cannot be used to describe the contact angle of a sessile drop on a rough or inhomogeneous surface like MOFs or MOF composites consisting of different materials because the force balance at the three-phase contact line is affected by surface roughness or inhomogeneities. More complex approaches taking roughness and heterogeneities into account are needed.

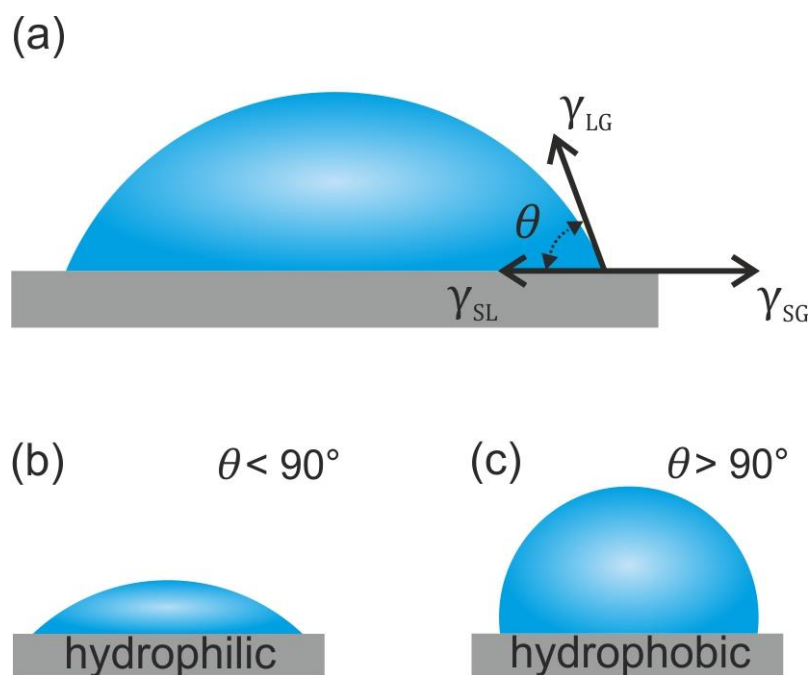


Figure 1. a) Schematic illustration of a sessile drop. The Young contact angle at the three-phase contact line depends on γ_{SG} the solid/gas-, γ_{SL} the solid/liquid-, and γ_{LG} the liquid/gas interfacial tensions. Sketch of a water drop on a hydrophilic surface (b) and on a hydrophobic surface (c).

2.2 Wetting of Rough Surfaces - The Wenzel Equation

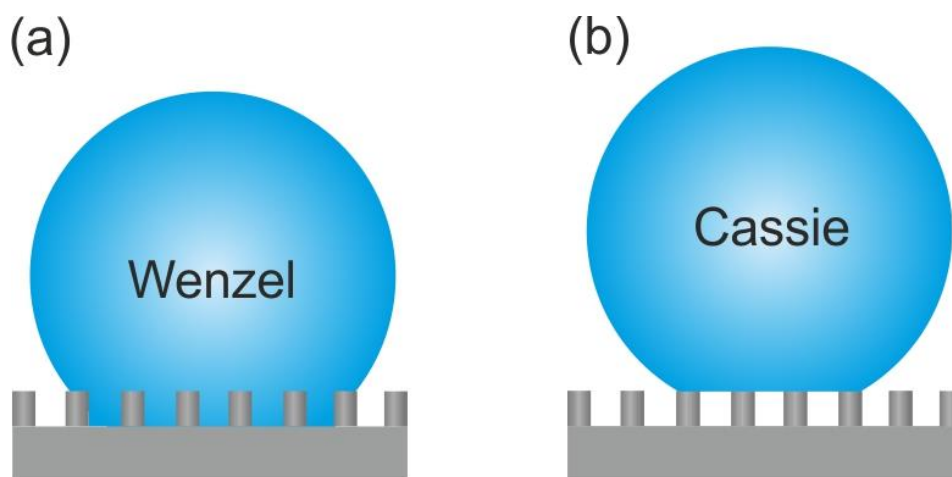


Figure 2. Different wetting states. a) Schematic representation of a droplet in the Wenzel state.^[119] b) Schematic representation of a droplet in the Cassie-state assuming a solid-liquid-air composite interface.^[120]

To account for surface roughness (**Figure 2a**), the roughness factor r was introduced by Wenzel.^[119] The roughness factor is the ratio of the actual surface area divided by the macroscopically apparent surface area and is thus larger than unity. The contact angle on a rough substrate is given by the Wenzel equation (Eq. 2):

$$\cos \theta_w = r \cdot \cos \theta \quad (2)$$

Here, θ_w is the apparent contact angle a drop forms on a rough surface, i.e. on a length scale much larger than the surface roughness or protrusions, and θ is the material's Young contact angle. In the Wenzel state, the liquid penetrates the rough surface's pores. The introduction of surface roughness amplifies the material's intrinsic wetting properties: it increases the contact angle if the surface is hydrophobic, and reduces the contact angle (or in extreme cases, causes complete wetting) if the surface is hydrophilic.^[104, 119] Note, the Wenzel equation does not permit that the roughness factor r exceed $1/\cos \theta$ because $\cos \theta_w$ would be greater than 1, otherwise.

2.3 Wetting of Heterogeneous Surfaces - the Cassie-Baxter Equation

If r would exceed $1/\cos \theta$, the drop takes the Cassie-Baxter state. In general, the so-called Cassie-Baxter-equation describe the wetting of composite surfaces consisting of different materials (Eq. 3):^[120]

$$\cos \theta_c = \sum_i \phi_i \cdot \cos \theta_i \quad (3)$$

Here, ϕ_i denotes the fraction of the total liquid-contacting surface that consists of material i , and θ_i is the intrinsic contact angle of material i . The Cassie-Baxter equation thus describes the apparent contact angle θ_c based on the surface's microscopic material composition. The so-called Cassie state is a situation in which a liquid droplet rests on the protrusions of a rough surface (Figure 2b) such that air is trapped beneath it. Indeed, if r would exceed $1/\cos \theta$, a solid-liquid-gas composite interface is thermodynamically favorable than wetting the rough structure in the Wenzel state. The Cassie state can be described by setting the value of i to 2 in Eq. (3), where $\theta_1 = \theta$ is the solid material's intrinsic contact angle and $\theta_2 = \theta_{\text{Air}}$ is the contact angle of a drop solely in contact with air ($\theta_{\text{Air}} = 180^\circ$). Eq. (3) reduces to:

$$\cos \theta_c = \phi_{\text{SL}} \cos \theta + \phi_{\text{Air}} \cos 180^\circ = \phi_{\text{SL}}(1 + \cos \theta) - 1 \quad (4)$$

Here, $\phi_{\text{SL}} = 1 - \phi_{\text{Air}}$ denotes the fraction of solid-liquid contact area.

It should be noted that the Young, Wenzel, and Cassie-Baxter equations all assume thermodynamic equilibrium between the three phases. Therefore, none of them can account for pinning events (see section 2.8), whose occurrence cause that the shape of a drop can no longer be described by a single contact angle, but the angle at the drop's front side differs from the angle at its back side (see section 2.8 for detailed discussion).^[102, 121-122]

2.4 Superhydrophobic surfaces

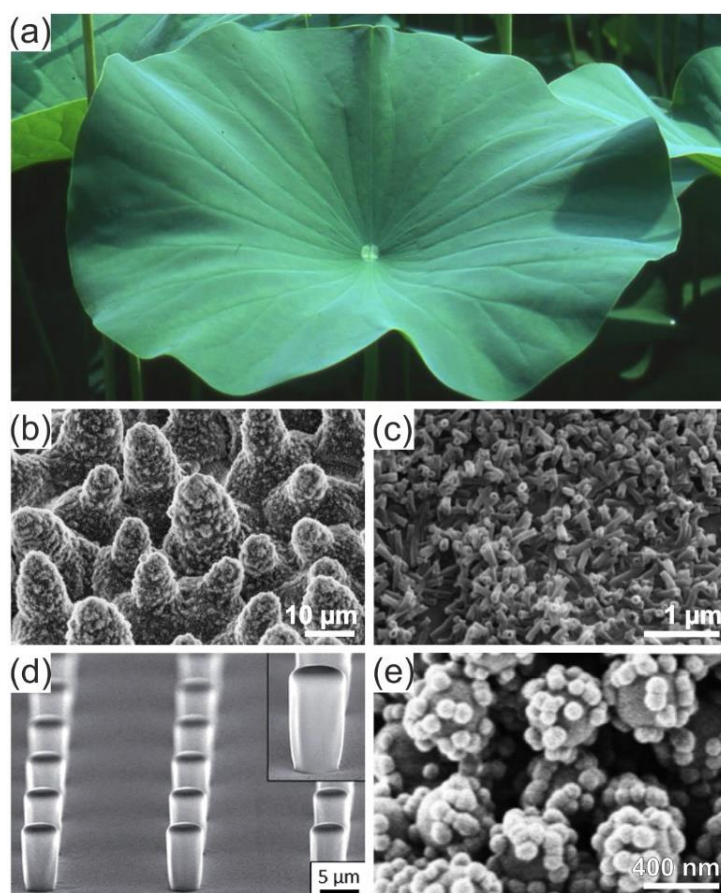


Figure 3. Natural and artificial superhydrophobicity. a) Photographs of a droplet on a lotus leaf b,c) Micro- and nanostructure of the lotus leaf observed by scanning electron microscopy (SEM). Reprinted from ref.^[123] Copyright 2011, Beilstein-Institut (CC BY 2.0). d) Model superhydrophobic surface consisting of SU-8 micropillar arrays. Reprinted from ref.^[124] Copyright 2014, Royal Society of Chemistry. e) Artificial lotus-like superhydrophobic surface consisting of raspberry-like nanoparticles. Reprinted from ref.^[125] Copyright 2011, Royal Society of Chemistry.

Hydrophobic surfaces on which drops adopt the Cassie state,^[120] and easily roll off while the surface is tilted by a few degrees ($< 10^\circ$) are known as superhydrophobic surfaces (Figure 3).^[121, 126-128] The mechanisms underpinning superhydrophobicity were not discovered until the late 1990s, when the biologist Barthlott and his coworkers analyzed the microscopic structure of the lotus leaf^[130]. These authors' groundbreaking publications prompted a substantial increase in academic and industrial research on natural and artificial superhydrophobic surfaces.^[126] Natural superhydrophobic surfaces are found on the leaves of various plants such as the lotus and the wings and body parts of some insects (e.g. the legs of water striders), among others (Figure 3a).^[130-131] Therefore, superhydrophobicity is often referred to as the lotus effect. Besides super-repellency, these surfaces are known for their exceptional self-cleaning properties.^[132-133] They have been used in applications including anti-icing,^[134-135] anti-biofouling,^[136-137] drag reduction,^[138-139] gas exchange,^[140-141] and oil/water separation.^[142-143] All surfaces of this type have two distinctive features: a high surface roughness on the micrometer or nano- scale and a low surface energy, i.e. a hydrophobic surface with an intrinsic contact angle of close to 90° or above. The liquid-solid contact area is low, often below 10% of the total composite interface. Consequently, water droplets generally adhere poorly to these surfaces and roll off easily. Shortly after the emergence of hydrophobic MOFs, the first superhydrophobic MOF surfaces were reported.^[112-113] These materials either have an intrinsically rough hydrophobic (micro-) structure^[151] or are formed by coating hydrophobic MOFs onto a rough substrate (for more details, see the synthesis section below).^[114]

2.5 Surface Tension and Energy

The interfacial tension γ can be interpreted as the work dW required to generate a new interfacial area dA (Eq. 5):

$$\gamma = \frac{dW}{dA} \quad (5)$$

It takes units of energy per area (J m^{-2}) or force per unit length (N m^{-1}). It should be noted that the term “surface energy” is preferred for solids but “interfacial tension” or “surface tension” are more commonly used for liquids.

Molecules in the bulk material are strongly attracted to one-another because of dispersion forces, electrostatic interactions, and hydrogen bonds. At the surface, some of these interactions are absent. Unlike molecules in the bulk material, surface molecules are not completely surrounded by other molecules of the same type. Therefore, the transport of molecules from the bulk to the

surface to decrease the material's surface area requires an input of energy to break intermolecular bonds. This energy is the surface energy. Liquids' surface tensions are generally between 20 and 80 mN m⁻¹.^[104] For instance, water has a surface tension of 72.5 mN m⁻¹ at 20 °C. However, some fluorinated liquids have surface tensions as low as 12 mN m⁻¹.^[152-153]

Liquid surface tensions are easily measured using with tensiometers utilizing a Du Noüy-ring^[154] or a Wilhelmy-plate or the sessile- or pendant drop method.^[104, 155] Measuring the surface energy of solids is less straightforward because the work required to deform a solid cannot easily be separated from that required to create new surface area. Therefore, surface energies are mostly measured indirectly. Most methods for determining a solid's surface energy rely on the measurement of contact angles for liquids with different surface tensions. Methods of this kind include the Zisman plot,^[156] Fowkes^[157], and Owens-Wendt-Rabel-Kaelble (OWRK)^[158-160] methods. However, these approaches are only applicable to materials with smooth, flat surfaces and cannot be applied to MOFs.

Solid surface energies can be as low as 6 mN m⁻¹ and as high as several thousand mN m⁻¹.^[161-163] Metals, metal oxides and glasses have large surface energies due to their strong (polar) intermolecular bonds, and can form strong interactions with polar liquids such as water. Conversely, low surface energy solids are non-polar. Consequently, the intermolecular interactions between water molecules are stronger than those between water molecules and the surface. Water droplets on such surfaces, subsequently have high contact angles to minimize the area of contact with the solid surface. Highly fluorinated surfaces have particularly low surface energies. An ideal surface fully covered with -CF₃ groups would have the lowest possible surface energy (6–7 mN m⁻¹)^[163]. Exchanging even one fluorine atom per -CF₃ group for hydrogen (-CF₂H) would raise the surface energy to 15 mN m⁻¹, and further exchange of fluorine for hydrogen would yield even higher surface energies (Table 1). It was also found that surfaces covered with terminal groups (-CF₃, -CH₃) have lower surface energies than their non-terminal counterparts (-CF₂-CF₂-, -CH₂-CH₂-).^[161]

Surface composition/Surface	Surface energy [mN m ⁻¹]
-CF ₃	6–7
-CF ₂ H	15
-CF ₂ -CF ₂ -	18
-CF ₂ -CH ₂ -	25
-CH ₃	20-24
-CH ₂ -CH ₂ -	31

-CH- (phenyl ring edge)	35
-CCl ₂ -CH ₂ -	40
Glass	250-500
Silicon	1100

Table 1. Surface energies for various surface compositions and surfaces at 20°C. ^[161-163]

Thus, to obtain low surface energies and high hydrophobicity, a surface or MOF material should have a high content of fluorocarbon compounds or at least large non-polar hydrocarbon fragments. Section 2.8 discusses how to synthetically incorporate low energy groups and fragments into MOFs.

2.6 Surface Energy Calculations by Inverse Gas Chromatography

Determining the surface energy of microcrystalline materials such as MOF powders is a major challenge in surface science. As noted above, the contact angles are influenced by surface roughness and the presence of micropores and micro cracks, which are difficult to control and can strongly affect measurement outcomes. Inverse gas chromatography (iGC) is an experimental technique that was pioneered in the 1950s and has matured into a widely used method for studying the surface properties of solids including rough materials such as MOFs.^[164-165] It is based on the dynamic exposure of a bed of powder to organic vapors. The vapors' retention times are measured, taking into account the temperature, vapor tension, and flow rate (Figure 4). It is assumed that the total surface energy γ_{SG} has two components: the dispersion γ_D and a specific/acid-base γ_{AB} component (Eq. 6).

$$\gamma_{SG} = \gamma_D + \gamma_{AB} \quad (6)$$

The measured net retention time corresponds to a specific net retention volume V , which is related to the free energy of adsorption ΔG_{ad} of a specific probe on the solid surface (Eq. 7):

$$-\Delta G_{ad} = RT \ln V + \text{const.} \quad (7)$$

Here, T the temperature and R is the universal gas constant. The const. term is related to a given reference state.^[165] The relationship between the dispersion component of the surface energy $\gamma_{D,SG}$ (γ_D for a solid-gas interface) and the net retention volume can be derived by noting that

the adhesion work W_a is related to the free energy of adsorption, applying Fowke's method (Eq. 8):^[157]

$$RT \ln V + \text{const.} = -\Delta G_{\text{ad}} = N_A r W_a = N_A r 2 \sqrt{\gamma_{\text{D,SG}} \gamma_{\text{D,LG}}} \quad (8)$$

Where $\gamma_{\text{D}} = \sqrt{\gamma_{\text{D,SG}} \gamma_{\text{D,LG}}}$. Here, N_A is the Avogadro constant, r the probe cross section, and $\gamma_{\text{D,LG}}$ the surface tension of the liquid probe. Using *n*-alkane probes, Schultz *et al.*^[166] showed that $RT \ln V$ depends linearly on $N_A r \sqrt{\gamma_{\text{D,LG}}}$, and Dorris & Grey^[167] demonstrated that $RT \ln V$ is linearly dependent on the alkane chain length (i.e. the number of carbon atoms, #C, in the chain). If $RT \ln V$ is plotted against $N_A r \sqrt{\gamma_{\text{D,LG}}}$ or #C using *n*-alkane probes (usually *n*-hexane, *n*-heptane, *n*-octane, and *n*-nonane), the dispersive surface energy γ_{D} can be determined from the slope of a linear fit of the resulting graph (Figure 4B). The specific/acid-base (γ_{AB}) component of the surface free energy can be determined by performing iGC experiments with a probe bearing an acidic and/or basic functional group. The specific γ_{AB} component of $-\Delta G_{\text{ad}}$ is derived by subtracting the dispersive component (determined using *n*-alkane probes) from the measured $RT \ln V$ for the specific acid-base probe (Figure 4C). By using a range of specific probes, one can study the surface's acid-base properties. It should be noted that various acid-base scales, and hence acid (γ_+) and base (γ_-) parameters, can be used for probes; commonly used scales include those of van Oss, Chaudhury and Good (vOCG)^[168], and Della Volpe^[169]. Results obtained using different scales may differ substantially. Consequently, calculated acid-base surface energy profiles should only be used for relative comparisons of the acid-base properties of similar materials.^[165] In addition, the measurements are performed at defined surface coverage (φ) values, making it possible to create profiles of γ_{D} (and γ_{AB} , γ_{T}) as a function of φ . Such profiles provide information about surface heterogeneity.^[170] γ_{D} values drop with increasing surface coverage because probes adsorb preferentially at sites of high surface energy, which usually correspond to structural or chemical surface defects. For instance, steps and cavities on the surface are high energy adsorption sites in graphite/multilayer graphene.^[171] The γ_{D} vs φ profile also scales with the size of graphene flakes^[172] and may provide valuable information that can be related to the material's rheological, structural, and (electro)catalytic properties.^[173] The iGC technique can also provide other important information about surface properties, including isosteric adsorption enthalpies and entropies, the adsorption energy distribution, and specific surface areas for various probes. Recent reviews have discussed these applications in detail.^[164-165, 170] Inverse GC measurements provides information about surface properties of powdered materials. The success of iGC in other fields

Hydrophobic Metal–Organic Frameworks, F. Geyer et. al. ,Adv. Mater. 2019, 1900820, DOI: 10.1002/adma.201900820

of material science suggests that it will be similarly useful for studying the surface properties of MOFs. In particular, it could be used to determine the surface energy of MOFs and its dispersion and acid-base components in order to estimate their interfacial tensions and hence their hydrophilicity/ hydrophobicity.

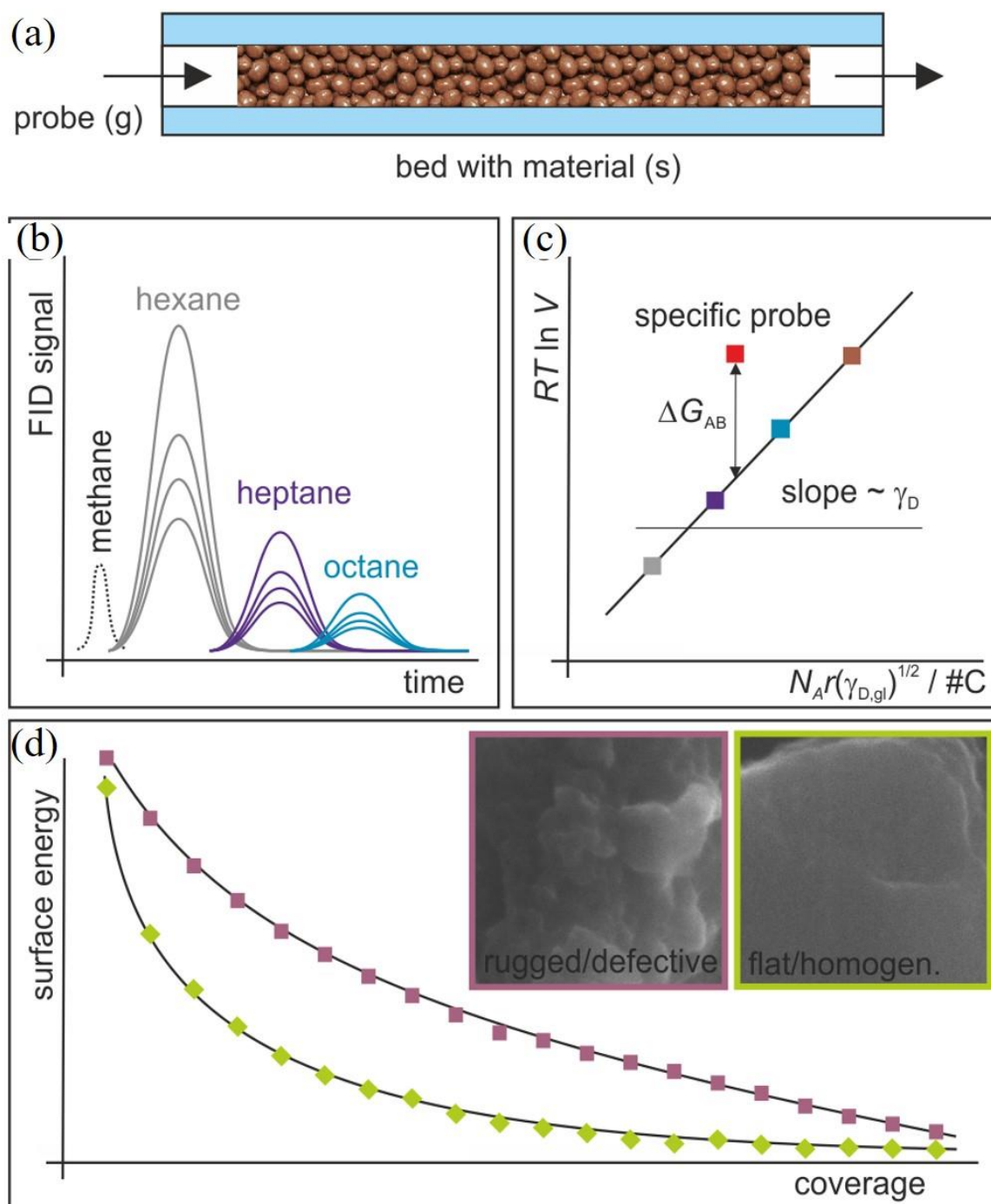


Figure 4. Probe vapors are passed through a bed of solid material in an iGC experiment (a). Net retention volume V is intended from the recorded chromatograms (b) and the dispersive γ_D and specific/acid-base γ_{AB} components of the surface energy were determined (c). The surface energy vs. surface coverage profile provides data on surface heterogeneity (d).

2.7 Contact Angle Measurements

Hydrophobic and superhydrophobic surfaces are typically characterized by performing contact angle measurements with a goniometer. A liquid drop is deposited on the surface and observed using a camera from the side. The drop profiles of static and moving drops are then recorded.^[174]

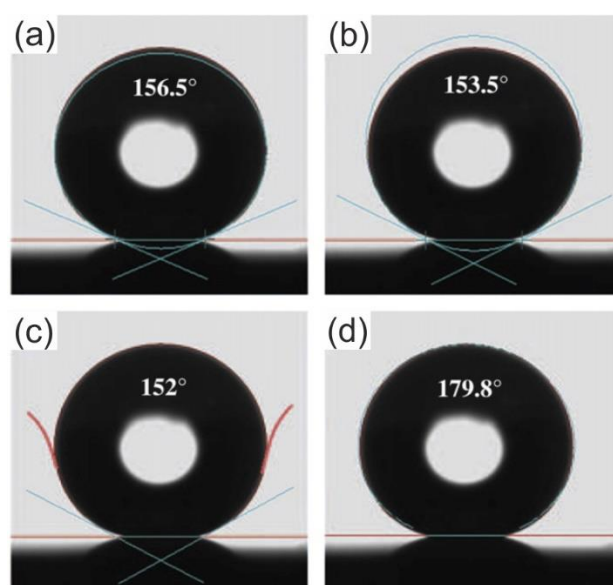


Figure 5. Side view of a sessile drop on a superhydrophobic surface. The lines show fits of the drop profile generated by a) Ellipse fitting, b) Circle fitting, c) Tangent fitting, and d) Young-Laplace fitting. The baseline is shown in red. The turquoise lines show the fitting result. Reprinted with permission from ref.^[175] Copyright 2008, Royal Society of Chemistry.

The contact angle is extracted from a fit of the drop profile. Figure 5 shows the fitting of a droplet using four common fitting methods: ellipse, circle, tangent, and Young-Laplace fitting. These methods yield very different results (ranging from roughly 150° to 180°) for the same recording.^[175] The circle and the Young-Laplace fits assume that the contact angles at the right and left side of the drop are identical. This is rarely true for rough surfaces because the three-phase contact line is pinned at protrusions. The elliptical and tangent fits permit different angles on the left- and right-hand sides of the drop profile. The tangent fit tries to match the slope of the meniscus close to the three-phase contact line. To reduce the effect of pinning of the drop to the surface of the needle, hydrophobic needles are recommended and the tip of the needle should be located approximately 1 mm above the surface. The camera settings can also influence the results; particularly important parameters include the illumination, brightness, contrast, and gamma. It is generally difficult to measure contact angles above 150° because the narrow gap between the liquid and the solid in such cases greatly reduces the amount of light

passing through the gap and hitting the camera, making it difficult to identify the real contact line. Conventional optical methods also typically cannot resolve details underneath droplets, such as whether the droplet is in the Cassie or Wenzel state.^[128, 175] This becomes even more severe for drop sizes above approximately 10 μL where gravity influences the drop's shape. It was recently shown that contact angles can be measured with greatly improved precision with techniques such as laser scanning confocal microscopy.^[176-177] Here, the lower side of the droplet is scanned using a laser. Reflected light at the liquid-air interface and as well as fluorescence from the bulk liquid is captured using detectors. A 2D or 3D representation of the droplet can be obtained. However, this technique requires a transparent substrate.

2.8 Contact Angle Hysteresis

On real surfaces with finite roughness and heterogeneity, one must discriminate between the so-called static, advancing, receding contact angles.^[178-179] The so-termed static contact angle (Young's, Wenzel or Cassie angle) depends on the way the drop is deposited on the surface, because of pinning at the three-phase contact line. Furthermore evaporation or slow spreading of the liquid results in changes of the static contact angle over time. For example, for MOFs it is important that the material is properly dried, and no humidity is adsorbed. Adsorbed molecules can change the surface energy or form a pre-wetting layer, and thus influence the contact angles. The static contact angle is thus not a clearly defined quantity despite its importance for surface characterization. The static contact angle lies between the advancing and receding contact angles, which can be measured using two methods. The first involves slow adding liquid to or removing liquid from a deposited droplet at a rate of around 0.5 mL min^{-1} or less (Figure 6).

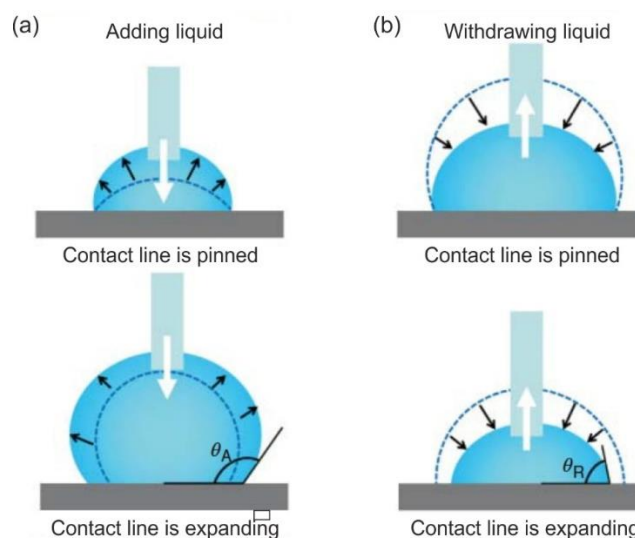


Figure 6. Advancing and receding contact angles can be measured by adding and removing liquid from a droplet. a) As liquid is added to the droplet, it expands and the contact angle increases. The contact line starts advancing when the contact angle exceeds the critical advancing contact angle. b) As liquid is removed from the droplet, it shrinks and the contact angle falls. The contact line starts receding when the contact angle falls below the critical receding angle. Reproduced with permission.^[180] Copyright 2017, Wiley-VCH.

As liquid is added, the droplet expands and its contact angle increases. When the contact angle reaches the advancing contact angle θ_{Adv} , the contact line advances. Similarly, as liquid is removed from the droplet, it contracts and its contact angle decreases until it reaches the receding contact angle θ_{Rec} and the contact line recedes. The difference among the advancing and receding contact angles is determined through contact angle hysteresis (CAH):^[174]

$$CAH = \theta_{Adv} - \theta_{Rec} \quad (9)$$

Another way to determine the advancing and receding contact angles is to deposit a droplet on a surface and gradually increase the surface's inclination, α (Figure 7a,b). At the moment immediately before the droplet starts to slide or roll down the inclined surface, the contact angles on the lower and upper sides of the droplet are equal to the advancing and receding contact angles, respectively. On a superhydrophobic surface such as a superhydrophobic MOF a 6 μ L sized water drop needs to roll off. Contrary, for a drop in the Wenzel state the adhesion of the drop on the surface is too high for it to roll off.

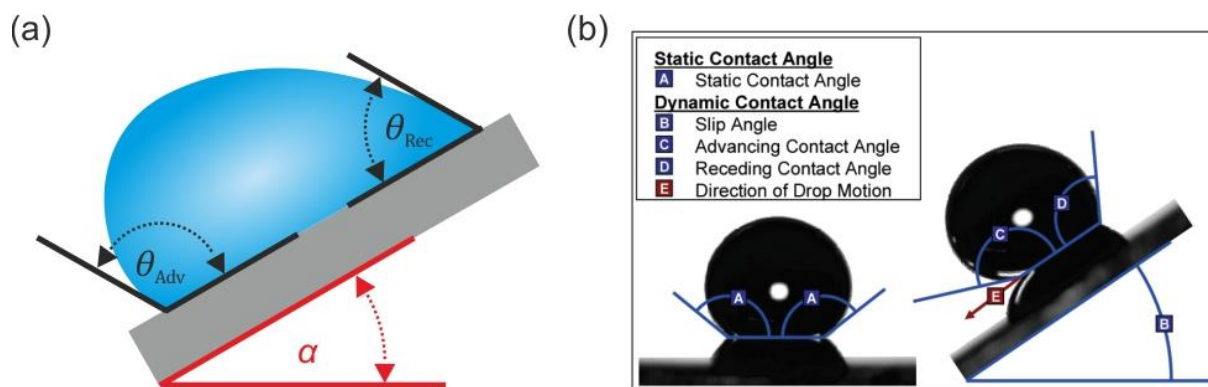


Figure 7. a) Illustration of a drop on a substrate tilted by the inclination angle α . The contact angles on the droplet's upper and lower sides are equal to the advancing and receding contact angles immediately before the droplet start to slide and as it is sliding. b) Experimental comparison between the static contact angle and the advancing/receding contact angles on an inclined substrate. Reproduced with permission.^[181] Copyright 2009, American Chemical Society.

Several factors and phenomena can cause contact angle hysteresis. One is surface roughness, whose effects can be explained by considering a simple case involving a droplet that is advancing over a surface with a microscopic protrusion or bump (Figure 8; left to right from Position A). The droplet advances with an intrinsic contact angle of 90° until it reaches the protrusion. It then “jumps” to the middle of the protrusion, where it can again assume the intrinsic contact angle of 90° (Figure 8; Position B). To advance further, the contact angle must exceed 90° . Therefore, the contact line remains pinned until the contact angle at the drop's front side exceeds θ_{Adv} . After overcoming the protrusion, the contact line can spread further, restoring its intrinsic contact angle of 90° . The same effect occurs for the receding contact line but in the opposite direction, leading to contact angles below 90° .^[104]

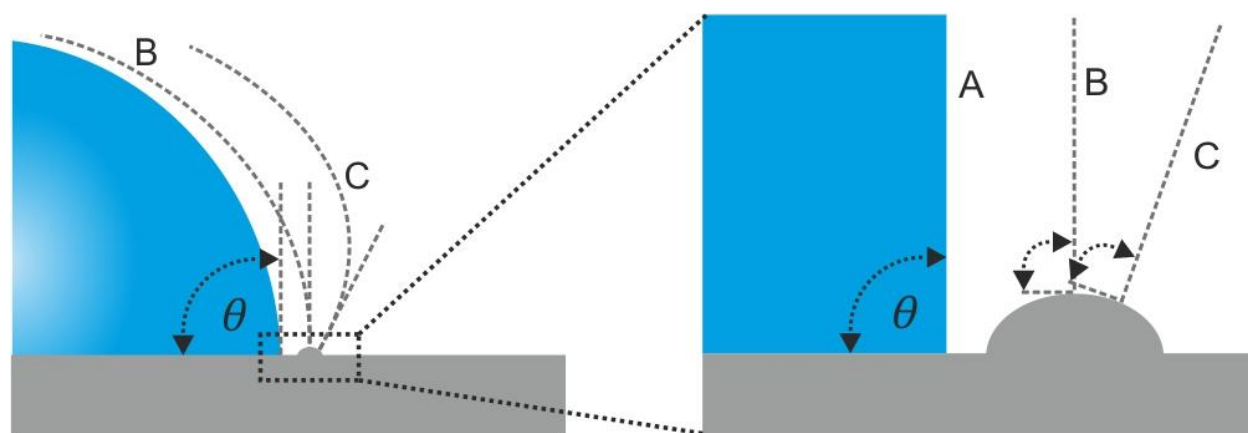


Figure 8. Illustration of a droplet advancing over a surface with a small protrusion (left side) and a more detailed view of the movement over the protrusion (right side). Adapted from ref.^[104]

Surfaces of different roughness may exhibit different levels of contact angle hysteresis. For surfaces in the Wenzel state, surface roughness greatly increases contact angle hysteresis, $\theta_{\text{Adv}} - \theta_{\text{Rec}} > 30^\circ$ (the example shown in Figure 8 resembles the Wenzel state).^[104] For superhydrophobic surfaces, i.e. those on which droplets exist in the Cassie-Baxter state, contact angle hysteresis is typically below approximately 20° .

Another cause of contact angle hysteresis is surface inhomogeneity (either structural or chemical). Like surface roughness, inhomogeneities can cause pinning of the contact line. The advancing contact line may be pinned on areas exhibiting a higher lyophobicity (liquid-repellency), whereas the receding contact line may be pinned in areas exhibiting a lower lyophobicity and thus a higher lyophilicity.

2.9 Roll-off Angle Measurements

In addition to contact angle measurements, roll-off angle experiments (sometimes called sliding angle experiments) are commonly conducted to determine a substrate's wettability.^[182-183] A droplet is deposited on the surface of interest, and the surface is then slowly tilted until the drop rolls off (Figure 7), which will occur if the droplet's adhesion to the substrate is low enough to be overcome by the gravimetric force acting on it. Therefore, the droplet volume affects the tilting angle. Volumes of 5 to 10 μL are typically used. It should be noted that the term sliding angle may be inappropriate because it has been shown that droplets do not slide but roll.^[184] Superhydrophobic surfaces,^[185] slippery liquid infused surfaces,^[186-187] and liquid-like surfaces^[188] all have low roll-off angles. The roll-off angle is related to the contact angle hysteresis according to the following equation (Eq. 9):^[184, 189-193]

$$F_{\text{RA}} = mg \sin \alpha = kw\gamma(\cos \theta_{\text{Rec}} - \cos \theta_{\text{Adv}}) \quad (9)$$

Here, m is the droplet's mass, g the gravimetric acceleration, and α the inclination of the surface (i.e. the roll-off angle). The factor k depends on the shape of the three-phase contact line and is usually taken to be 1.^[184] The contact width w of the droplet is measured perpendicular to the

droplet's movement. The contact angle hysteresis appears in the $(\cos \theta_{\text{Rec}} - \cos \theta_{\text{Adv}})$ term. Consequently, a low contact angle hysteresis will generate a low roll-off or sliding angle. Roll-off angle measurements have the advantage of being fast and more reproducible than contact angle measurements because they do not depend on the lighting and the choice of baseline and require no fitting. Because of the better reproducibility of the roll off angle compared to measurements of the contact angles, we recommend to use α to characterize superhydrophobic MOFs. However, it is important that the drop's volume is listed too.

3 Synthesis of Hydrophobic MOF Materials

Considerable research effort has been dedicated to the synthesis of numerous pristine hydrophobic metal-organic frameworks and composites, as shown in Figure 9. This section reviews the strategies that have been used to prepare these materials. The first approach involves decorating the ligands of the MOF with hydrophobic fluorine-containing and/or (long-chain) alkyl substituents linkers to alter the MOF's surface properties (Figure 9a). This strategy promotes stability in liquid water by creating a hydrophobic outer surface that inhibits the diffusion of water molecules into the pores of MOF. The second approach involves so-called post-synthetic strategies, like hydrophobic responsive groups are grafted onto pre-formed MOFs (Figure 9b).

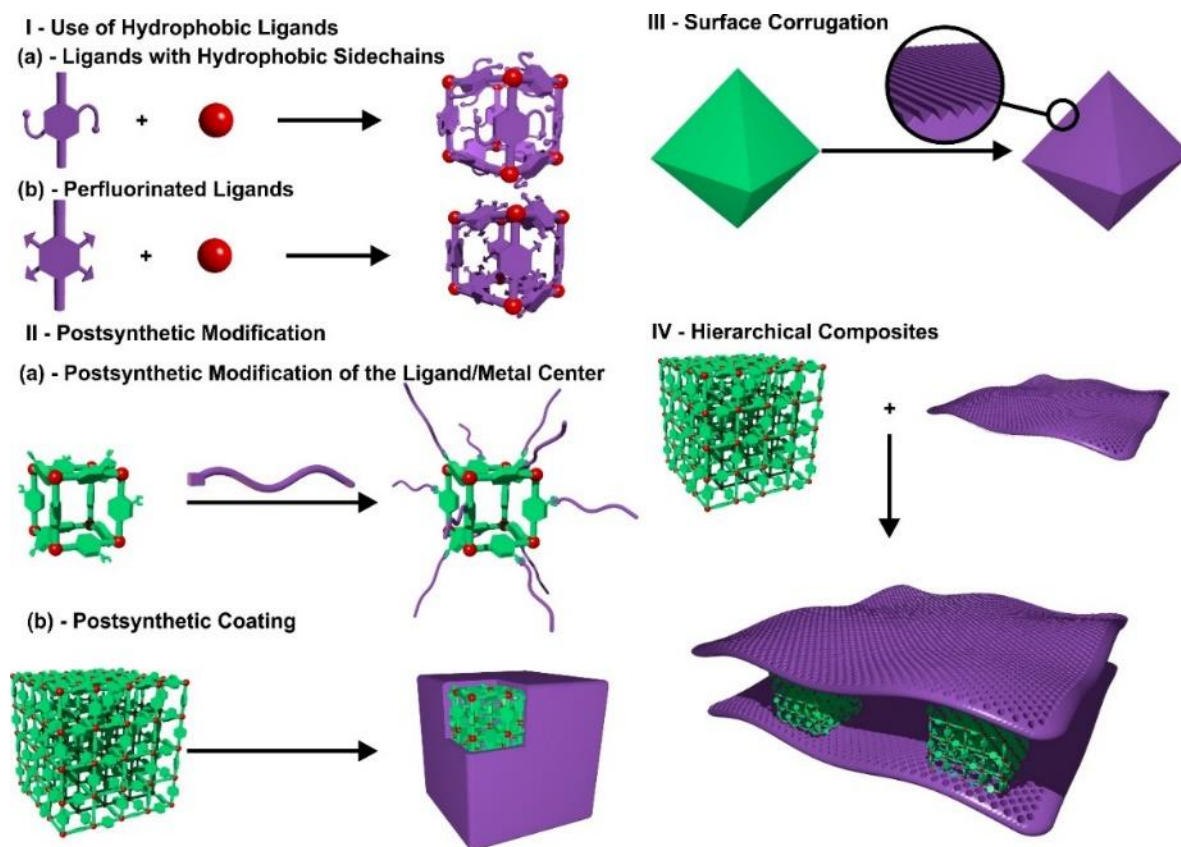


Figure 9. Strategies for fabricating hydrophobic MOFs and composites.

Although both strategies can effectively exclude water from the MOF's pores, they also render the inherent porosity of resultant MOFs, largely inaccessible because of the steric bulk groups on the ligand/outer surface. An alternative approach that generates highly hydrophobic outer surfaces but preserves internal porosity involves creating high nano-to micrometer surface roughness (Figure 9c). Although this approach is facile and applicable to many MOFs, it has mainly proved effective with microporous materials; reports describing its successful application to mesoporous MOFs are scarce. The most common way of synthesizing mesoporous MOFs involves using large organic linkers, but such frameworks often suffer from low thermal and mechanical stability as well as self-catenation. Consequently, there is a clear need to develop rational methods for fabricating robust hierarchical hydrophobic MOFs with tailored structures and wetting surface areas. One way to avoid the limitations associated with tailoring the functional properties of hydrophobic MOFs solely by varying the combinations of nodes and linkers, their topology, and the linker design is to make hybrid MOFs using other 2D graphene materials. The final approach involves the synthesis of hierarchical micro-mesoporous composites based on the hybridization of microporous MOFs intercalated with

Hydrophobic Metal–Organic Frameworks, F. Geyer et. al. ,Adv. Mater. 2019, 1900820, DOI: 10.1002/adma.201900820

hydrophobic two-dimensional layers/membranes (Figure 9d). After the initial steps of the development of different hydrophobic MOF materials and composites, recent studies on hydrophobic MOFs have focused on some critical challenges in the measurement of hydrophobicity by various methods, and the issues they create in practical applications.

3.1 Linker-Based Hydrophobic Metal–Organic Frameworks

Eddaoudi and coworkers introduced the principle of isorecticular synthesis in 2002.^[194] This principle states that frameworks with identical topologies but different functionalities pinned to the ligand backbone can be prepared by using ligands having different functionalities but identical connectivity. Since then a plethora of different ligands have been prepared and used for the de novo synthesis of MOFs with tailored properties. Among other things, this approach has been used to introduce acidic sites or metal-chelating groups for catalysis, to modulate gas adsorption properties, or to confer flexibility.^[195-196] However, the attachment of overly large groups often alters the framework's topology. There have been some efforts to induce hydrophobicity by incorporating ligands that are perfluorinated, possess fluorinated or alkyl side chains, or simply increase the surface corrugation and energy. The preparation of ligands with alkyl chains and the use of perfluorinated ligands to construct MOFs has been explored by several groups. However, there are few reports describing the attachment of perfluorinated sidechains, and very few in which the use of such sidechains was a central aspect of the report. Some representative hydrophobic ligands are listed in Table 2.

In 2011, Omary and coworkers described superhydrophobic fluorous metal–organic frameworks (FMOFs) whose internal pores were linked with CF_3 groups.^[65] This confers remarkable air- and water-stability. The authors reported two hydrophobic MOFs, FMOF-1 (Ag_4Tz_6) and FMOF-2 (Ag_3Tz_4), based on 3,5-bis(trifluoromethyl)-1,2,4-triazolate (Tz) organic linkers containing flexible CF_3 groups (Figure 10a). The hydrophobicity of FMOF-1 was determined by water adsorption and comparison with the porous materials zeolite-5A and (Figure 10c). Zeolite-5A shows significant water adsorption at a very low P/P_0 value (<0.1), and is thus hydrophilic but BPL carbon shows little uptake up to $P/P_0 = 0.4$. Once after that it shows significant uptake at $P/P_0 = 0.8$ with a typical type V hysteresis loop, which confirms its hydrophobic behavior. However, FMOF-1 shows little uptake of water, even at saturation pressure. It indicates the large channels (1.2×0.8 nm) of FMOF-1 are inaccessible to water adsorption. Despite this, the material exhibited significant uptake of benzene, cyclohexane, *n*-hexane, toluene, and *p*-xylene, demonstrating its hydrophobicity (Figure 10b). FMOF-1 retains its PXRD pattern even after soaking in water for several days, confirming its structural stability.

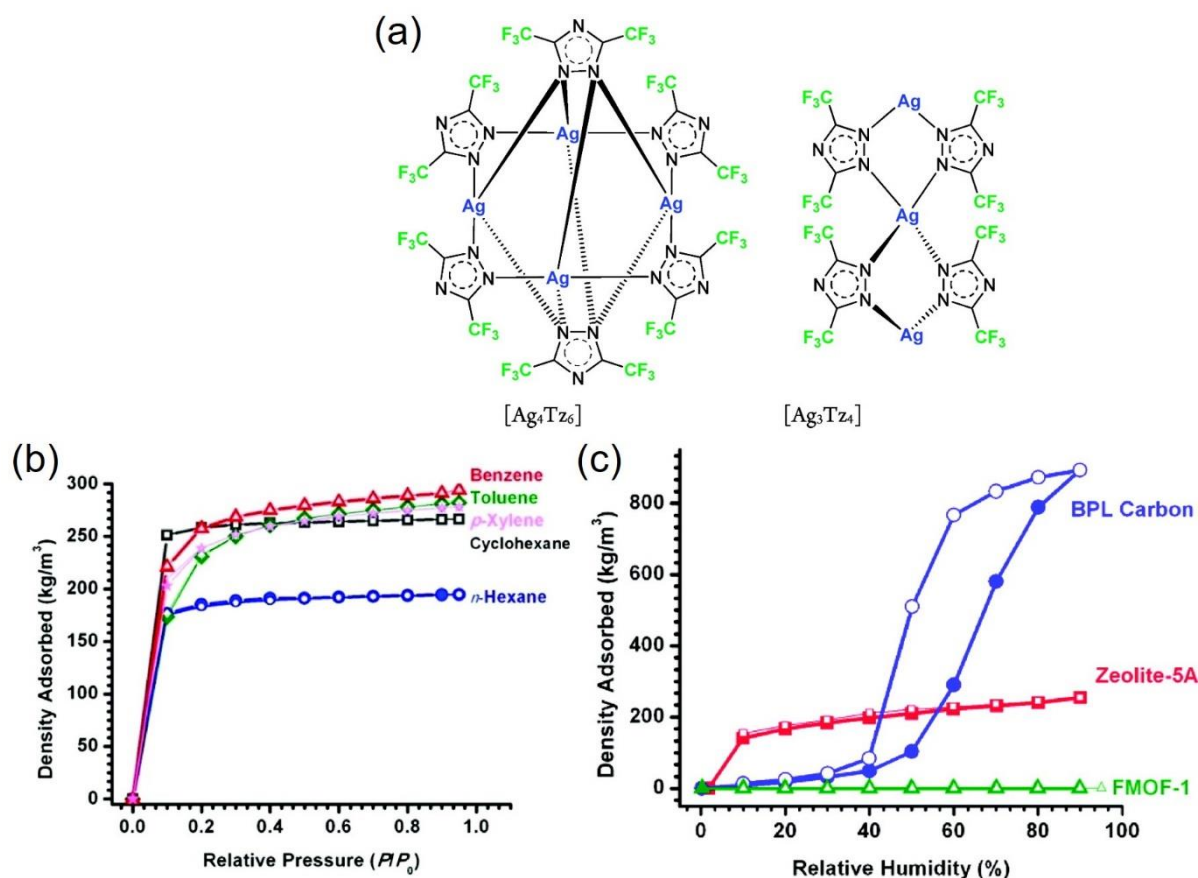


Figure 10. (a) Building units of resultant fluorinated MOFs FMOF-1 and FMOF-2; (b) Organic solvent benzene, cyclohexane, *n*-hexane, toluene-*p*-Xylene adsorption of F-MOF-1; (c) Water adsorption isotherms of BPL carbon, Zeolite-5A, FMOF-1. Reproduced with permission from ref.^[65] Copyright 2011, American Chemical Society.

In 2013, Miljanić reported three perfluorinated Cu_2 paddlewheel MOFs incorporating the perfluorinated ligands $H_2OFBPDC$ (2,2',3,3',5,5',6,6'-Octafluorobiphenyl-4,4'-dicarboxylic acid) and $H_2PFBPTZ$ (5,5'-(Perfluorobiphenyl-4,4'-diyl)bis(1H-tetrazole)) (Figure 13a).⁹³ Two frameworks using the $H_2OFBPDC$ ligand were prepared, MOFF-1 ($Cu_2(OFBPDC)_2(MeOH)_2$) and MOFF-2 ($Cu_2(OFBPDC)_2(DABCO)$).^[89] The structures of these frameworks are shown in Figure 11a; note that DABCO = diazabicyclo [2.2.2]octane. MOFF-1 is prepared by combining $H_2OFBPDC$ with $Cu(NO_3)_2$ under solvothermal conditions. Single crystal XRD experiments revealed the formation of square grids of 2D $Cu_2(OFBPDC)_2$ layers capped by MeOH. The layers are aligned in a staggered fashion, with the Cu_2 paddlewheels above the void space of the adjacent layers, as also occurs in the non-fluorinated material MOF-118 (Figure 11b). MOFF-2 features

similar $\text{Cu}_2(\text{OFBDC})_2$ layers that are interconnected by DABCO pillars, generating a three-dimensional framework (Figure 11c). Performing the same synthesis using the tetrazole-based linker H_2PFBPTZ results in the formation of $\text{Cu}(\text{PFBPTZ})(\text{H}_2\text{O})$. The bridging of $\text{Cu}(\text{H}_2\text{O})$ chains by the tetrazolate ligands in this framework gives rise to 1D channels similar to those seen in the dicarboxylate-based MOFs MIL-47 and MIL-53 (Figure 11d). To estimate the hydrophobic/philic properties of MOFs **1–3**, their water contact angles were measured before and after solvent removal from the pore space. MOF-1 has water contact angles of 0° and $108 \pm 2^\circ$ before and after solvent removal, respectively. MOF-2 crystallizes without solvent in the pore space and has a H_2O contact angle of $151 \pm 1^\circ$. Finally, MOF-3 has very similar contact angles of $134 \pm 1^\circ$ and $135 \pm 2^\circ$, in the solvated and desolvated states, respectively.

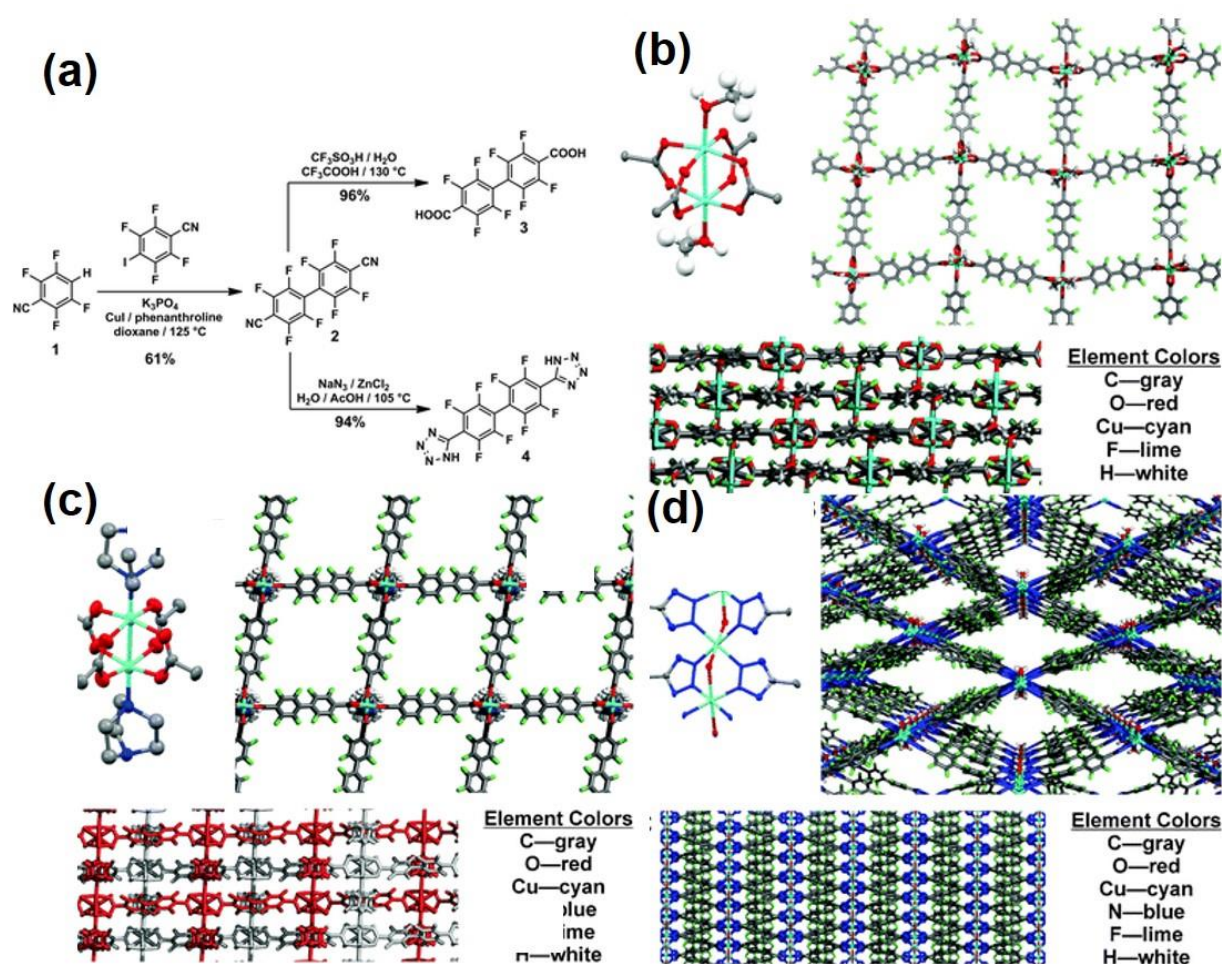


Figure 11. a) Synthesis of ligands **3** and **4**. Depiction of the secondary building units, and crystal structures of b) **MOF-1** ($\text{Cu}(\text{OFBDC})(\text{MeOH})$), c) **MOF-2**, ($\text{Cu}_2(\text{OFBDC})_2(\text{DABCO})$) and **MOF-3** ($\text{Cu}(\text{PFBPTZ})(\text{H}_2\text{O})$). Reproduced with permission from ref.^[89] Copyright 2013, Royal Society of Chemistry.

In 2016, Maji and co-workers reported, the superhydrophobic nanoscale coordination polymer $\text{Zn}(\text{OPE-C}_{18})(\text{H}_2\text{O})_2$ (**NMOF-1**) using long octadecoxy based organic linker as oligo-(*p*-phenyleneethynylene)dicarboxylate (**OPE-C₁₈**) and Zn^{II} (Figure 12a).^[151] Using several characterization methods, the authors showed that this material forms 3D supramolecular framework via van der Waals interactions between adjacent C_{18} alkyl chains. To investigate the hydrophobic behavior of NMOF-1, the authors performed benzene and water adsorption isotherms at room temperature. (Figure 12b). Further NMOF-1 have superhydrophobic behaviour and water contact angle is around 162° and further it is supported advancing and receding contact angle measurements (Figure 12c-e).

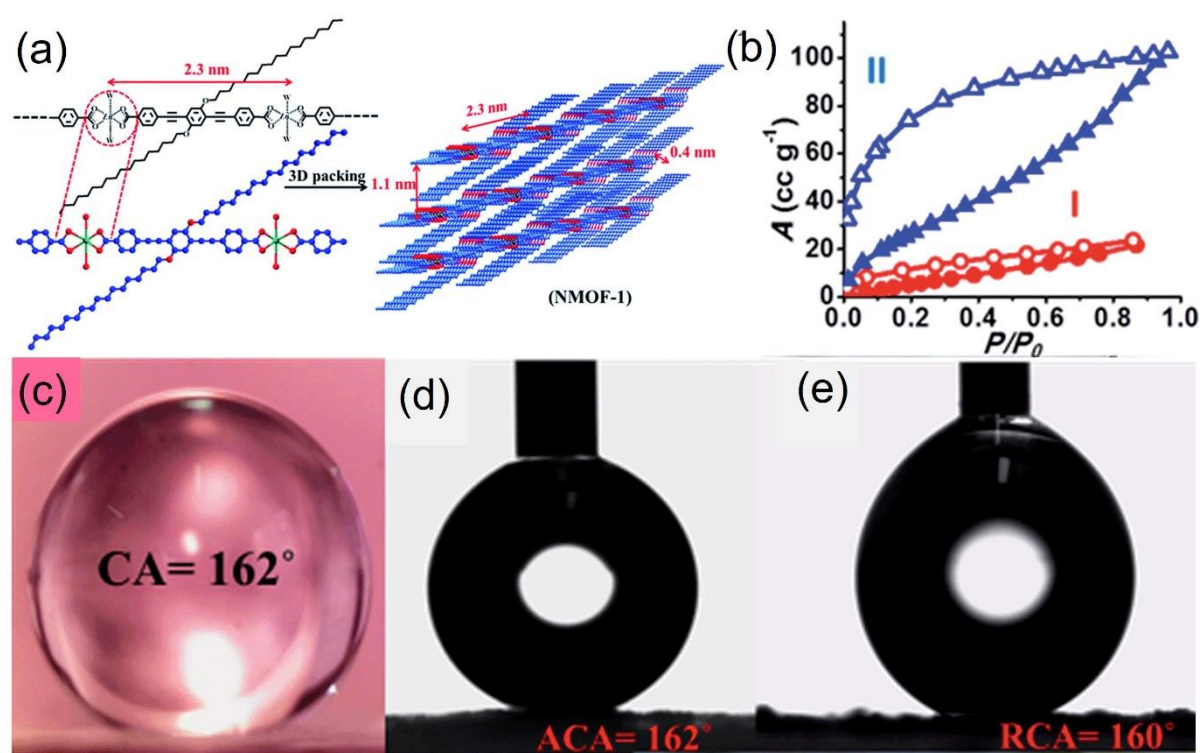


Figure 12. a) Synthesis of NMOF-1 comprised between Zn^{2+} and OPE-C_{18}^{2-} . (b) Solvent adsorption isotherms of NMOF-1 where water (red circles) and benzene (blue triangles) measured at 298 K. The material was coated on glass substrates and the resulting water contact angle amounts to 160–162° (circle fitting mode) (e-g). Reproduced with permission from ref.^[151] Copyright 2016, Royal Society of Chemistry.

Sun and coworkers also reported a superhydrophobic MOF named **UPC-21** ($\text{Cu}_3(\text{PEIP})_{1.5}(\text{H}_2\text{O})_3$), comprised with a pentyptycene-based 4,4'-(Pentyptycene-6,13-diyl-bis(ethyne-2,1-diyl)isophthalic acid (H_4PEIP) and copper nitrate under solvothermal conditions (Figure 13a).^[197] The framework's structure features six PEIP^{4-} ligands connecting twelve Cu_2 paddlewheel SBUs to generate a $\text{Cu}_{24}(\text{PEIP})_6$ tubular cage in which six paddlewheel SBUs arrange on the equator and three Cu_2 PWs

form triangular bottom and top faces (Figure 13 b). Many of the benzene rings of PEIP^{4-} project into the cage and providing a hydrophobic cavity. The spindle-shaped cages are interconnected, giving rise to a 3D porous framework. The contact angles for **UPC-21** are $145 \pm 1^\circ$, suggesting a highly hydrophobic/oleophilic character owing to its multi-aromatic carbon units in the framework (Figure 13c). Contact angle measurements were performed by placing water dropwise onto the surface of **UPC-21** via syringe. If a substrate bearing UPC-21 powder was inclined after placing a droplet of water on its surface, a UPC-21-covered water droplet (a “liquid marble”) was formed; this is known to be a common occurrence with hydrophobic powders. The authors also measured UPC-21’s contact angles with crude oil diluted with hexane. The oil was adsorbed rapidly, confirming the material’s oleophilicity (Figure 13d).

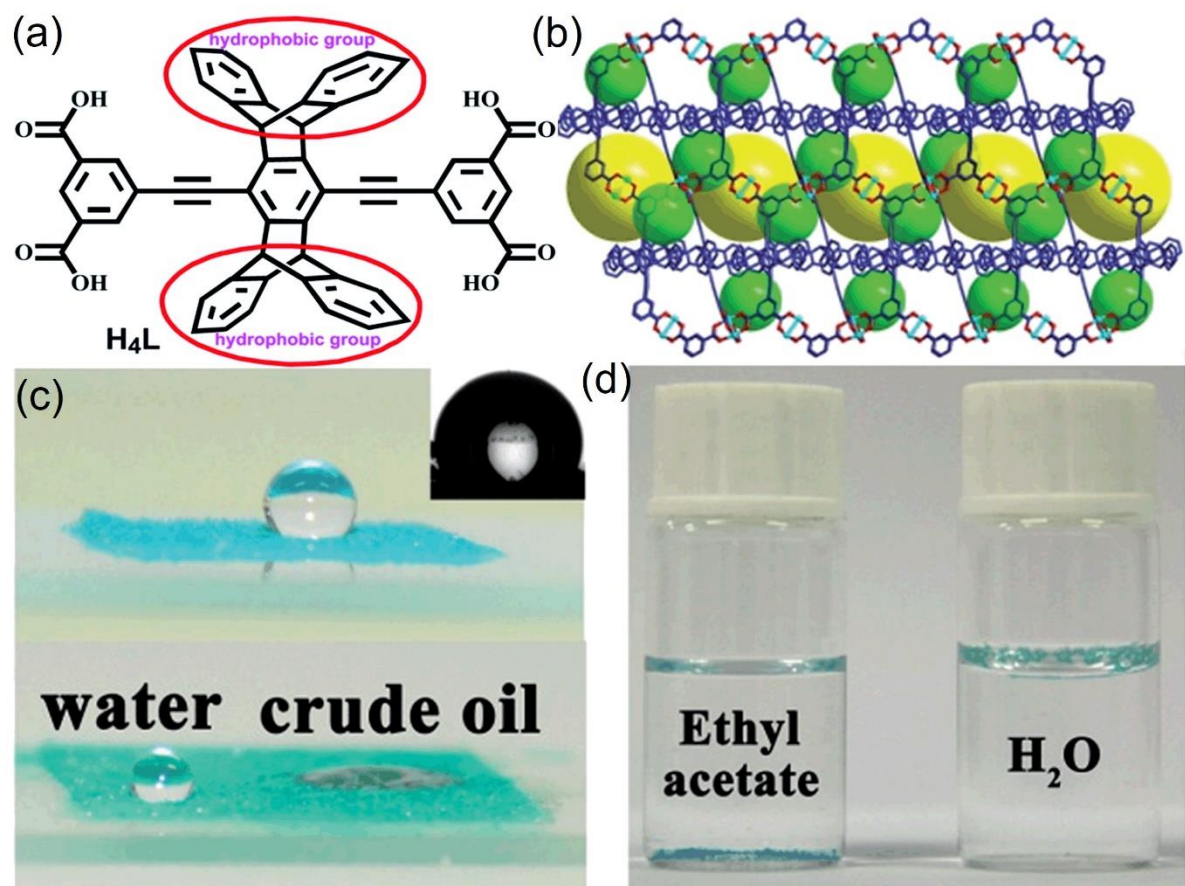


Figure 13 a) Structure of ligand, 4'-(Pentiptycene-6,13-diyl-bis(ethyne-2,1-diyl))isophthalic acid (H_4PEIP) of **UPC-21**; b) View of 3D porous framework constructed with spindle-shaped cage originated from six PEIP^{4-} and twelve Cu_2^{4+} paddlewheel SBUs. (c) top, optical image of water droplet shows its superhydrophobic behaviour; bottom, quick oil uptake of MOF reveals oleophilic

nature e) The MOF UPC-21 sinking in ethyl acetate and floating in water Reproduced with permission from ref.^[197] Copyright 2016, Royal Society of Chemistry.

3.2 Induction of Hydrophobicity by Post-synthetic Modification

Another way to enhance the stability of moisture or water sensitive MOFs is functionalization hydrophobic fluorine and/or alkyl/aromatic groups. This approach has the advantages that synthetic pathways to known MOFs can be used and that some of their properties are retained when their wettability is changed. Two variants of this approach can be distinguished: functionalization with organic substituents and coating with a protective hydrophobic layer. The first variant requires a framework bearing reactive positions, either in the form of reactive substituents on the ligand that can undergo organic reactions under mild conditions (e.g. $-NH_2$ or $-N_3$ substituents that can undergo amidation or click reactions, respectively) or the existence of coordinatively unsaturated metals, that permit the installation of organic molecules (e.g. via solvent-assisted linker installation). The second variant entails adding polymeric layers over the outer surface of the MOF and requires that the material be stable towards the coating. While both methods can substantially increase moisture resistance, they have the disadvantage of substantially changing the framework's porosity.

In 2011, Cohen and coworkers reported the introduction of hydrophobicity into the otherwise moisture-labile IRMOF-3 ($Zn_4O(NH_2-BDC)_3$) via postsynthetic modification.^[74] The exposed framework's amino groups were esterified with various carboxylic acid anhydrides with different alkyl chain lengths and degrees of branching. The parent frameworks IRMOF-1 ($Zn_4O(BDC)_3$) and IRMOF-3 are hydrophilic, with water contact angles of $\sim 0^\circ$ (Figure 14a). Functionalization with acetic anhydride (IRMOF-3-AM1), propionic anhydride (IRMOF-3-AM2), or butyric anhydride (IRMOF-3-AM3) also yielded hydrophilic materials with contact angles of $\sim 0^\circ$. However, functionalization with valeric anhydride, which has a longer OCC_4H_9 side chain, yielded the material IRMOF-3-AM4, which has a contact angle above 116° and is thus moderately hydrophobic. The stability of these samples was assessed by performing powder XRD measurements after exposure to ambient air (Figure 14c). The non-functionalized IRMOF-1 exhibited a striking decrease in crystallinity after just 1 day, together with the formation of a parasitic phase, MOF-69c.

The inclusion of hydrophobic units increases stability of IRMOF structure in open atmosphere. Further, the powder XRD patterns of the amidated derivatives remained even after four days, with no other additional peaks and its intensity. The applicability of this methodology

to other systems was confirmed by transferring it to the MIL-53(Al) (Al(OH)(BDC)) structure. The amine-tagged MIL-53(Al)-NH₂ (Al(OH)(NH₂-BDC)) was modified by using three various alkyl anhydrides as MIL-53(Al)-AM1, -AM4, and -AM6. The contact angle measurements shows unfunctionalized MIL-53(Al), MIL-53(Al)-NH₂, and MIL-53(Al)-AM1 were all hydrophilic (contact angles ~ 0°) and functionalized MIL-53(Al)-AM4 and MIL-53(Al)-AM6 possess superhydrophobic behaviour (contact angles above 150°).

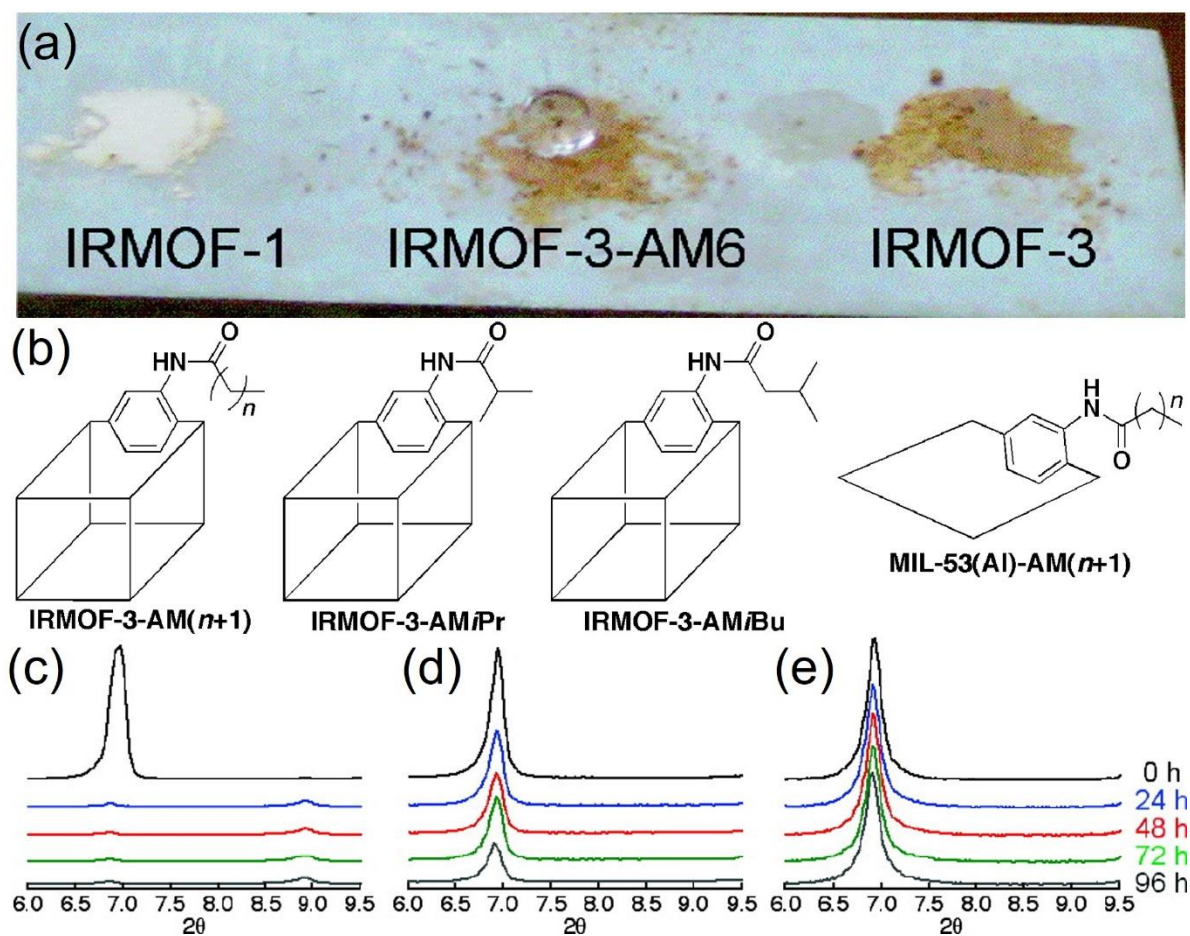


Figure 14. a) Optical image of **IRMOF-1**, **IRMOF-3-AM6** and **IRMOF-3**, where water droplet dropped on the crystals of corresponding MOFs; (b) Schematic representations of the MOFs prepared via PSM. (c) powder XRD patterns over period of four days (c) **IRMOF-1**; (d) **IRMOF-3**; (e) **IRMOF-3-AM15** Reproduced with permission from ref.^[74] Copyright 2010, American Chemical Society

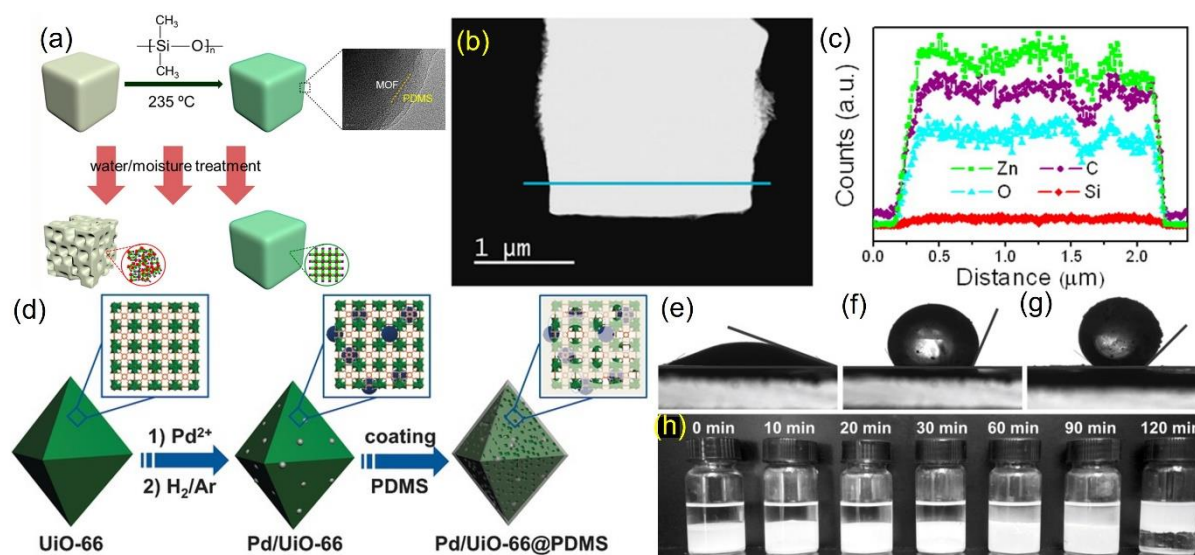


Figure 15. (a) Schematic representation of postsynthetic medication of MOF with PDMS coating (b-c) Line-scan profile of PDMS coated MOF-5crystal; (c) PDMS surface modification of Pd/Uio-66, where Uio-66 MOF encapsulated with Pd nanoparticles; water contact angles of (e) Pd/Uio-66, (f) Pd/Uio-66@PDMS-10, (g) Pd/Uio-66@PDMS-20; (h) optical image of hybrid Pd/Uio-66@PDMS-T dispersed in water–ethyl acetate mixture at different durations. Reproduced with permission.^[62, 81] Copyright 2014, American Chemical Society; Copyright 2016 Wiley

In 2014, S. Hu and coworkers reported post-synthetic route by modifying the surfaces of MOF materials with hydrophobic polydimethylsiloxane (PDMS) to enhance their water and moisture resistance using a facile vapor deposition technique (Figure 15a).^[62] The volatile PDMS precursor (PDMS stamp) is placed in a reactor with the pristine MOF powder, resulting in the formation of a hydrophobic PDMS coating. The authors took three representative MOFs having three different secondary building units (SBUs) as IRMOF-1 with $\text{Zn}_4\text{O}(\text{COO})_6$ clusters, HKUST-1 ($\text{Cu}_3(\text{BTC})$; $\text{H}_3\text{BTC} = 1,3,5\text{-benzenetricarboxylate}$) with paddle wheel $\text{Cu}_2(\text{COO})_4$ centers, and $\text{Zn}_2(\text{BDC})_2(\text{DABCO})$ with pillared paddlewheels $\text{Zn}_2(\text{COO})_4\text{N}_2$ clusters. IRMOF-1, HKUST-1, and $\text{Zn}_2(\text{BDC})_2(\text{DABCO})$ are all hydrophilic and water-sensitive, with water contact angles close to 0° . However the PDMS-coated represented MOFs all exhibited water contact angles of $130 \pm 2^\circ$, demonstrating their hydrophobicity. It should be noted that, the hydrophobic behaviour of these represented MOFs remained same even after exposure to open atmosphere. To verify the presence of the PDMS layer on these representative MOFs, the element distribution of PDMS-coated IRMOF-1 was studied by acquiring a composition line-scan profile (Figure 15 b-c). It shows the silica surface homogeneously distributed throughout the surface of MOF, with a Si/Zn atomic ratio of $\sim 4.1\%$.

Further, SEM micrographs revealed that IRMOF-1 crystals have a regular cubic morphology with smooth surfaces. However, after standing in a humid environment for two days, the material exhibited severe deterioration. N₂ sorption experiments yielded results in good agreement with the above observations. Interestingly, the coated crystals retained their morphology under the same conditions. The BET surface areas (S_{BET}) of pristine and PDMS coated IRMOF-1 were calculated to be 3118 and 3159 m²/g, respectively. In 2016, Jiang and coworkers used this PDMS coating procedure to modify the surface hydrophobicity of Pd/UiO-66 (Zr₆O₄(OH)₄(BDC)₆), a composite containing a MOF and stabilized Pd nanoparticles (NPs) (Figure 17 c).^[81] The stability of the composite before and after PDMS coating was characterized by powder XRD and BET measurements. The water contact angle of Pd/UiO-66 is 25°, where the contact angles increased significantly upon PDMS coating 115° and 140° (Figure 15e-h).

3.3 Introduction of External Surface Corrugation by the Use of an Hydrophobic Unit

Despite improving the moisture or water stability of MOFs, the approaches described above have important drawbacks such as reduced porosity, tedious synthetic procedures, or a need for complex instrumentation. Another important strategy for creating highly hydrophobic exterior surfaces while retaining internal porosity by creating significant upon PDMS coating rough surface of nano-to-micrometer length scale. In 2014, Kitagawa and coworkers reported superhydrophobic MOF materials by using external surface corrugation originated from aromatic surface groups.^[51,53] These authors reported a porous coordination polymer with external surface design (PESD), [Zn₄(μ₃-OH)₂(BTMB)₂(DMF)₃(MeOH)] using organic linker BTMB = 1,3,5-tris(3-carboxyphenyl)benzene), which possesses terminating hydrocarbon aromatic surface (Figure 16a-b). CO₂-adsorption data indicate that this material's surface area is 295 m² g⁻¹, demonstrating its porosity and guest accessibility. The powder XRD measurements of flake-shaped single crystals of PESD-1 confirmed that preferential orientation along the [0 k 0] direction and it is revealing the (010) surface to be the dominant surface. Further AFM characterization showed (010) flat surface is micro to nano meter length scales (Figure 16c-d). To examine the material's hydrophobic properties, contact-angle measurements were performed on as-synthesized and activated powder, single crystals and pellets, all of which yielded markedly different results (see discussion in challenges in contact angles). The authors also measured solvent adsorption water, benzene, cyclohexane and, toluene, at 298 K.

Hydrophobic Metal–Organic Frameworks, F. Geyer et. al. ,Adv. Mater. 2019, 1900820, DOI: 10.1002/adma.201900820

Interestingly, the water adsorption isotherm experiments on PESD-1 revealed unusual adsorption behavior for a hydrophobic material, with two significant steps at 0.27 and 2.3 kPa on the adsorption isotherm. This indicates that while the exterior surface is repellent towards liquid water, the interior pore space is actually hydrophilic and accessible to water vapor (like a lotus leaf). The adsorption isotherm of organic solvents as toluene and benzene shows a gate-opening adsorption isotherm, but cyclohexane was not adsorbed. These results indicate that PESD-1 have frame work flexibility along with size-selective pores toward guest molecules. The same group recently reported a *de novo* synthetic method for preparing other MOF composites, including PESD-2 and -3, $[\text{Zn}_2\text{M}_2(\mu_3\text{-OH})_2(\text{BTMB})_2]$ ($\text{M} = \text{Co}$ and Ni), with Co^{2+} or Ni^{2+} occupying the octahedrally-coordinated Zn^{2+} positions.^[198] The oxo-clusters in the pristine phases of PESD-2&3 \supset Guest are replaced by $[\text{Zn}_2\text{M}_2\text{O}]^{6+}$ ($\text{M} = \text{Co}$ and Ni) clusters. It should be noted that the reported bimetallic composites exhibit outstanding superhydrophobic behavior even at high temperature. PESD-2(Co) exhibits a particularly large surface area and good uptake of solvents such as benzene, toluene, and cyclohexane.

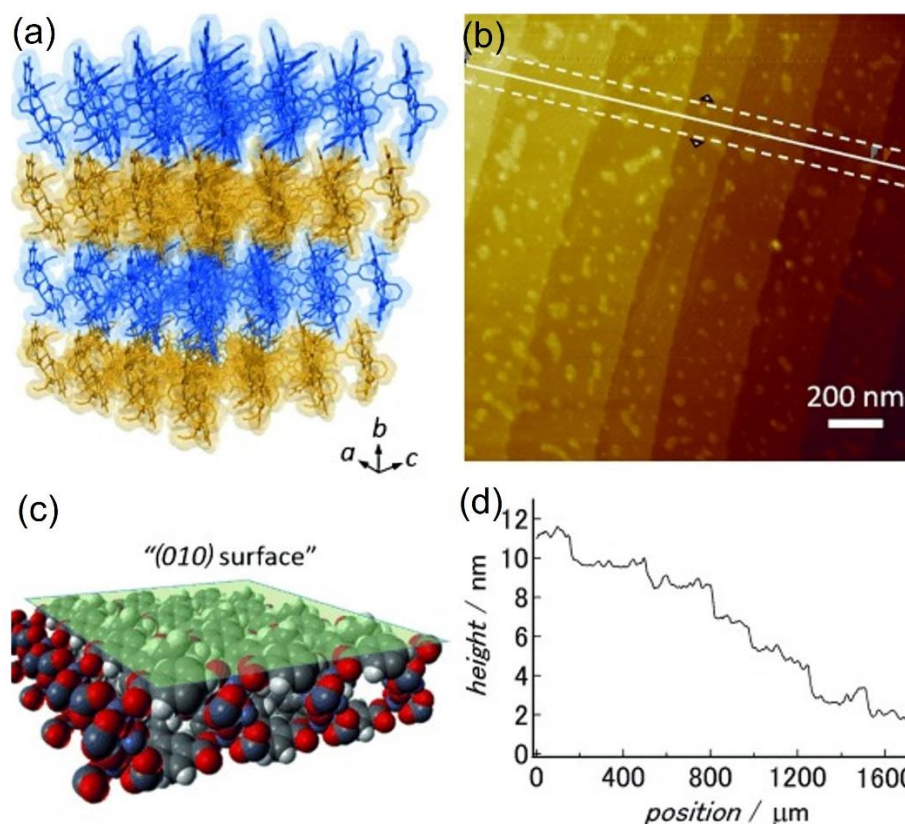


Figure 16. a) 3D stacking of individual 2D layers, b) AFM image of the (010) surface of **PESD-1** \supset Guest c) the low surface energy termination of the (0k0) surface. d) Average topographic

profile extracted from the AFM micrograph exhibiting a terrace structures with widths from 100–400 nm. Reproduced with permission.^[53] Copyright 2014 Wiley-VCH.

In contrast, among zeolite imidazole framework (ZIFs) family, the ZIF-8 (2-me IM, 2-methyl imidazole) is hydrophobic pore surface due to its free flexible methyl groups but a hydrophilic crystal surface. Where The ethyl imidazole based ZIF -[Zn(eim)₂] (MAF-6, Metal-azolate framework) shows an exceptionally hydrophobicity on both internal pore and external crystal surfaces along with high thermal and chemical stability.^[60] To study the internal hydrophobic pore surfaces of MAF-6, solvent adsorption isotherms were performed at RT. The MAF-6 shows significant uptake of methanol, ethanol and benzene as 13.27, 9.15 and 6.36 mmol g⁻¹. Where the adsorption isotherm of ethanol and methanol shows typical type-V and benzene have type-IV adsorption isotherm and it conclude hydrophobic behaviour of MAF-6. The contact angle of MAF-6 shows around $143 \pm 1^\circ$ due to large basins located on the (100) crystal surface that originate from its nearly mesoporous cavities. Therefore, the hydrophobicity of MAF-6 originated from highly corrugated crystal surface on the nano meter- scale.

3.4. Hydrophobic MOF Composites:

Despite the large number of hydrophobic MOFs based on fluorinated and long alkyl chain ligands, a great deal of research has been devoted to fabricating porous MOFs with hierarchical pores (both micro and meso), high surface areas, and large pore volumes. Hierarchical porous hydrophobic MOF composites can be synthesized by growing MOF nanoparticles on various fluorine-based graphene layered materials. Our group recently reported the synthesis of various MOF composites with fluorographene (FG). FG was used in the preparation of these composites because it allows functional groups to be incorporated into the basal plane of graphene rather than at the edges of the layers.^[199-200] Highly fluorinated graphene oxide (HFGO) was combined with zeolitic imidazole frameworks (ZIFs) under solvothermal conditions (Figure 17a) to produce an MOF composite, HFGO@ZIF-8, with superhydrophobic-superoleophilic properties.^[114] The powder XRD of this hybrid featured all planes corresponding to pristine ZIF-8 (Zn(mIm)₂). Interestingly, its nitrogen adsorption isotherms exhibited both type-I and type-IV shapes, indicating the presence of micropores (presumably originating from ZIF-8) and mesopores (due to the stacking of ZIF-8 nanocrystals over HFGO layers), respectively. The hybrid has a BET surface area of 590 m²/g. Pore size distribution calculations using the NLDFT method suggest a distribution extending over both

the microporous and mesoporous regimes (2-3 nm). An XPS analysis of HFGO@ZIF-8 confirmed that the nature of its fluorinated groups was unaffected by the synthetic process, i.e. the pendant covalent C-F groups of HFGO were retained in the composite. These results indicate that the ZIF-8 nanocrystals act as pillars intercalated between HFGO layers by selective nucleation and controlled growth over oxygen functional groups, producing a hierarchical porous structure. Furthermore, the $-CF_3$ termination of the HFGO layers gives the composite a very low surface energy (Figure 17a), which is another prerequisite for hydrophobicity. Remarkably, contact angle measurements showed that the composite's water contact angle (162°) exceeds those of pristine ZIF-8 and HFGO (56° and 125° , respectively; see Figure 17b-d). These results illustrate the interplay between two features – a hierarchical structure and a low surface energy – that make surfaces hydrophobic. Additionally, the composite took up oil droplets very rapidly (within 15 s); its oil contact angle is essentially 0° , indicating superoleophilicity (Figure 17e).

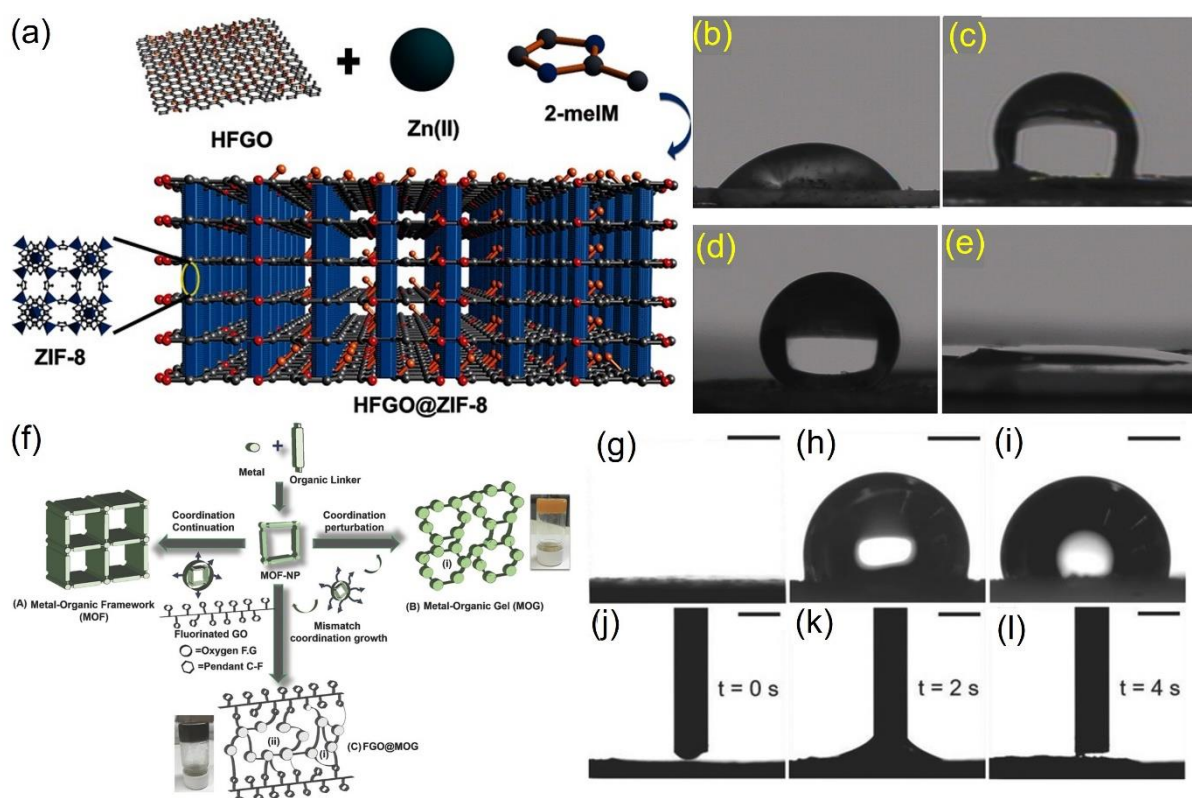


Figure 17. a) Schematic illustration for making hybrid **HFGO@ZIF-8** where HFGO =highly fluorinated graphene oxide, ZIF-8; Zn(meIM)₂ meIM=methyl imidazole. photo graphs showing (b) water contact angle of ZIF-8 as 56° and (c) water contact angle of HFGO is 125° (d) water contact angle of **HFGO@ZIF-8** hybrid 162° and (e) oil contact angle of 0° ; (f) N₂ adsorption isotherm of **HFGO@ZIF-8** showing hierarchical porous behaviour, and in set shows the pore size distribution calculated from NLDFT method (g) Schematic illustration of the formation **FGO@MOG**; Photographs o (h) pristine MOG; (i) pristine FGO, (j)

Hydrophobic Metal–Organic Frameworks, F. Geyer et. al. ,Adv. Mater. 2019, 1900820, DOI: 10.1002/adma.201900820

FGO@MOG, (k–m) and time dependent hexadecane contact angles on **FGO@MOG** (n) N₂ adsorption isotherms of **FGO@MOG** . Reproduced with permission.^[114] Copyright 2016 and 2017 Wiley-VCH.^[85]

In a continuation of this work, we reported the economically viable and readily scalable preparation of hydrophobic-oleophilic porous gels by simple mixing of hybrid composites of metal-organic gel (MOG) composed of Al(III) ions and 1,3,5-benzene dicarboxylate linkers (BTC) and fluorinated graphene oxide (FGO) under solvothermal conditions (Figure 17 f).^[85] PXRD analyses of the composites indicated that their crystallinity was low, as only a few broad diffraction peaks were observed. Nevertheless, the data indicated that the material's structure is closely related to that of MIL-100(Al). The **FGO@MOG** exhibits a typical type-IV N₂ adsorption/desorption isotherm, proves meso/macro porous nature with pore diameters of 2-70 nm . This demonstrates that hierarchical (micro/meso) pore structures can be obtained by using fluorinated graphene oxide (FGO) to disrupt MOF crystal growth, promoting mismatched growth over oriented crystallization. It should be noted that the MOF nanoparticles initially go through controlled nucleation and nanoparticles selectively coordinated with the oxygen functionalities of the FGO sheets. The composite's hydrophobicity was assessed by measuring its advancing/receding contact angles (Figure 17 g-l). The advancing water contact angle of hybrid is $126^{\circ} \pm 4^{\circ}$, showing its hydrophobic behavior. Pristine FGO and MOG exhibit advancing water contact angles of $116^{\circ} \pm 4^{\circ}$ and 0° , respectively. Its hexadecane contact angle was close to 0° , confirming the hydrophobic-oleophilic behavior of the **FGO@MOG** composite. At the same time, hydrophobic-oleophilic composites based on a hydrophobic MOF incorporated in a graphene oxide (GO)/sponge composite were presented by H.L. Jiang and coworkers.^[48] The used MOF USTC-6 (Cu₂HFPD) uses a tetra carboxylate organic linker H4HFPD (4, 4'-(hexafluoroisopropylidene) diphthalic acid) with a Cu₂ paddlewheel SBU, prepared under solvothermal conditions (Figure 18a). Single crystal XRD analysis reveals, 2D layers in the *ac* plane with a wave-like surface with exposed pendant -CF₃ groups between the 2D layers, which lesser the surface energy and induce the high hydrophobicity of USTC-6 . The powder XRD data further confirm phase purity and more importantly preferential orientation along the (060) plane. The water contact angle measurement show angles of up to 132° for the crystals. Further, for the preparation of an oil-spill up cleaning device, the authors incorporated the obtained hydrophobic MOF on branches sponges functionalized with GO. The GO surface has oxygen functional groups like carboxylic, hydroxyl and epoxy, which facilitate anchoring of USTC-6. The composite shows water contact angles in the range of 121° – 130° and oil droplets quickly adsorbs into this sorbent. The hydrophobic/oleophilic

Hydrophobic Metal–Organic Frameworks, F. Geyer et. al. ,Adv. Mater. 2019, 1900820, DOI: 10.1002/adma.201900820

nature of USTC-6 is transferred to the device, and the incorporation of USTC-6 changes the properties of GO@Sponge (Figure 18b) . In a similar manner, Ghosh and coworker reported a hydrophobic MOF membrane UHMOF-100/PDMS/PP (UHMOF= ultra-hydrophobic MOF, PP- poly propylene fabric). UHMOF ($\text{Cu}_2(\text{BTFPADB})_2$) comprises of the fluorinated linker $\text{H}_2\text{BTFPADB}$ (4,4{[3,5 - bis(trifluoromethyl)phenyl] azanediyldibenzoic acid) in presence of copper nitrate.^[94]

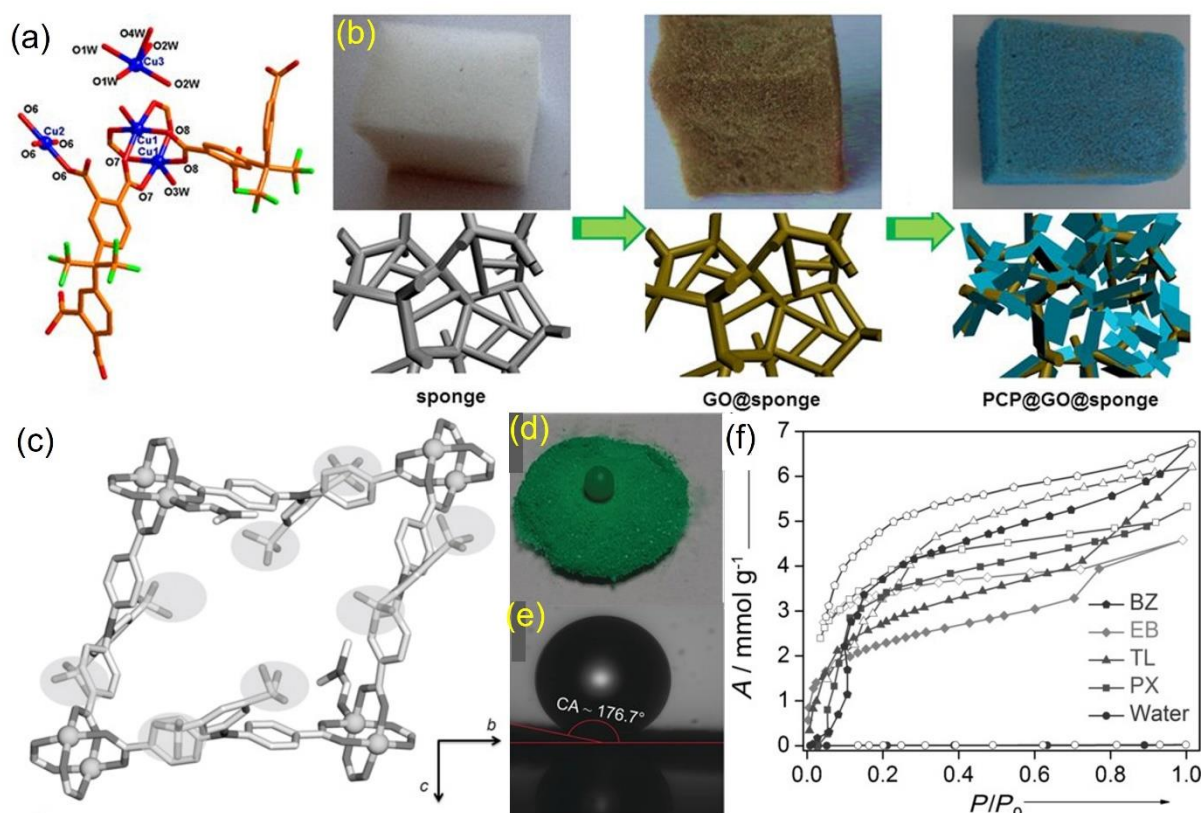


Figure 18. (a) Fluororous based organic linker of MOF USTC-6. (b) Schematic illustration of the synthetic route towards USTC-6@GO@sponge and photographs confirming the well-retained morphology of the sponge; (c) A single fluororous pore of UHMOF-100; (d) Water droplet suspended on UHMOF-100 crystallites. (e) Image of a water drop slowly cast on the water-repellent surface of the UHMOF-100 pellet with a CA of about 176°, resembling mercury-like droplets. (f) Hydrocarbon vapor sorption isotherms of Benzene, Ethyl benzene, Toluene and para-Xylene compared to water. Reproduced with permission. Copyright Wiley VCH 2016^[94] and Nature^[48]

Single crystal XRD analysis shows a 2D grid-based framework structure with ultramicropores decorated with bis(trifluoromethyl) moieties (Figure 18c). To examine super hydrophobicity behavior of UHMOF, contact angle measurements were conducted, with a water contact angle

Hydrophobic Metal–Organic Frameworks, F. Geyer et. al. ,Adv. Mater. 2019, 1900820, DOI: 10.1002/adma.201900820

of 177° and an oil contact angle of 0, indicating superoleophilicity (Figure 18d-e). The authors recorded vapor sorption isotherms at 298 K. Due to the hydrophobic pores, the water adsorption isotherm showed no uptake (Figure 18 n.) In case of hydrophobic organic vapor molecules significant uptake is observed, particularly for common oil components (i.e. C_6 – C_8 hydrocarbons) such as benzene (BZ), ethyl benzene (EB), toluene (TL), and *p*-xylene (PX) (Figure 18f). To utilize the properties of UHMOF-1, it was integrated into a device, by spray-coating the MOF onto a PDMS/PP membrane. The water contact angle of the prepared membrane amounts to 135° highlighting the hydrophobic nature of the fabricated MOF membrane.

3.4 Challenges in characterization of hydrophobic MOFs

Determining and characterizing MOFs' hydrophobicity is challenging because standard methods such as contact angle measurements are often not readily applicable; there is a lack of unified and universal standard methods and protocols. The challenges can be illustrated by considering the example of a specific hydrophobic MOF, namely (PESD-1) $Zn_4(\mu_3\text{-OH})_2(\text{BTMB})_2$ (Figure 19).^[53] This framework is based on the aromatic linker molecule H_3BTMB (benzene-1,3,5-tris(*m*-benzoic acid)) and is obtained in the form of single crystals with dimensions of 1–3 mm. Consequently, the surfaces of MOFs made from these crystals have a very high roughness. Water droplets deposited on this MOF adopt near-spherical shapes and can roll off at $\approx 10^\circ$ (Figure 19a). This demonstrates that the MOF is intrinsically hydrophobic (i.e., its intrinsic contact angle is $> 90^\circ$), as otherwise the water would spread in accordance with the Wenzel equation. Upon grinding the crystals, a powder with a smaller grain size ($< 10\ \mu\text{m}$) is obtained. This powder is still sufficiently rough for deposited water droplets to adopt a high static contact angle ($> 150^\circ$) and a spherical shape (Figure 19b). After degassing the ground MOF powder to remove guest molecules (the grain size remains $< 10\ \mu\text{m}$; Figure 19c) and pressing it into a pellet, the static contact angle declines markedly, to $\approx 110^\circ$. This indicates that a single MOF material can exist in at least four different states, each with different hydrophobicities. How then should we measure its behavior and what factors should be taken into account when doing so?

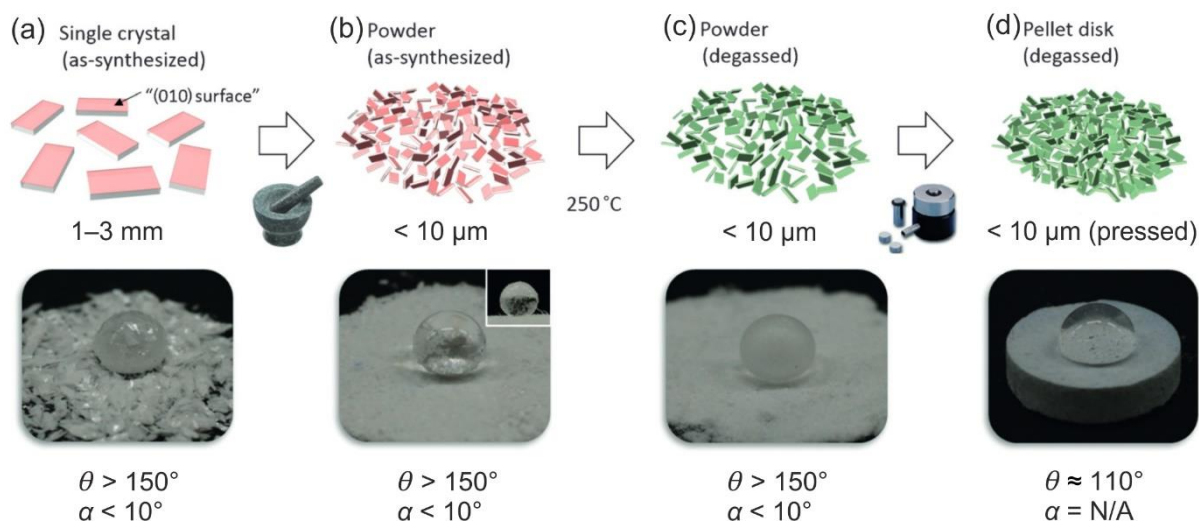


Figure 19. A typical hydrophobic MOF material [PESD-1]. a) Crystalline state with a large crystallite size of 1-3 mm; a deposited water droplet adopts a near-spherical shape. b) Grinded powder with a smaller grain size of $< 10 \mu\text{m}$ and a similar water contact angle. c) Degassed powder retaining the $< 10 \mu\text{m}$ grain size. d) Powder pressed into a pellet, reducing surface roughness and contact angles. Reproduced with permission.^[53] Copyright 2014, Wiley-VCH.

Most MOF materials and composites are obtained in the form of crystals or powder.^[112-113] However, in some cases, a MOF may be coated on a substrate such as a glass.^[202] The treatment of the crystals or powder prior to the contact angle measurement is crucial because the substrate's roughness significantly affects the wetting properties, as discussed in Section 2.2-2.4. Therefore, one can only meaningfully compare the measured contact angles of different MOF materials if their pretreatment was identical. Pressing a powder into a pellet disk significantly reduces its surface roughness and thus alters its wetting properties, allowing assessment of its intrinsic hydrophobicity.

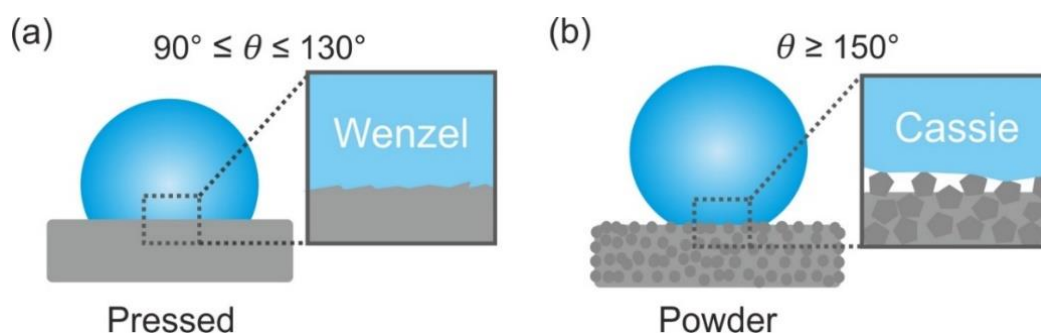


Figure 20. a) Schematic illustration of a water droplet on a hydrophobic MOF powder pressed into a tablet adopting the Wenzel state. b) Water drop on hydrophobic MOF powder without further treatment. Air is entrapped underneath the droplet (Cassie state) between the powder grains due to the high surface roughness of the powder.

Depending on the applied pressure and the powder's characteristics, some residual roughness remains. Because of the reduced roughness, water droplets resting on top of the pressed tablet should exist in the Wenzel state, with a contact angle between 90° and 120° (but potentially up to 130° depending on the remaining roughness and the material's intrinsic contact angle; Figure 20a). The highest possible water contact angle on an ideally flat nonporous substrate is 120° , which can only be achieved by perfluorinated ($-\text{CF}_3$) surfaces.^[156, 163] Only the introduction of roughness can enhance the contact angle above 120° . Contact angles for bare powders can substantially exceed this limit because of their high roughness, which depends mainly on the crystallites' grain size. In many cases, the roughness due to the grain size is sufficient to support a Cassie state (Figure 10b). In such cases, the drop rests on the topmost powder grains and air is trapped beneath it. In such cases, the droplet may have a contact angle above 150° and be able to roll off (which will occur at inclinations below 10° for 5–10 μL water droplets). The observed contact angle thus largely depends on the surface morphology and structure, i.e. the grain size and arrangement. Consequently, a material of high intrinsic hydrophobicity could have a lower observed contact angle in the Cassie state than a material with a lower intrinsic hydrophobicity but more suitable roughness. Powder-based measurements are also error-prone because powders are loose assemblies of grains that are easily “picked up” by droplets, potentially reducing the air-water interfacial tension. This is why it is difficult to measure contact angle hysteresis on MOF powders. The advancing contact angle can be measured with reasonable accuracy by increasing the droplet volume, but the removal of liquid to measure the receding contact angle can cause the droplet to pick up powder grains, which strongly influences the measurement and may lead to the formation of a “liquid marble”.^[203-205] Therefore, it is inadvisable to measure contact angle hysteresis on powders; such measurements should ideally only be performed on pressed pellet disks. The load needs to be listed.

Contact-angle based methods for measuring the surface energy of MOF materials such as the Zisman plot^[156] or OWRK methods^[158-160] are unreliable because even pressed tablets exhibit residual roughness, and the MOF material is likely to adsorb the low surface tension liquids (alkanes, oils, alcohols) used in those methods due to the inherent porosity of the MOFs. Instead methods such as iGC (section 2.6) should be used to measure the surface energy. As noted above, the characterization of hydrophobic MOFs is very challenging. We therefore wish to offer a few suggestions that may help in the development of standardized protocols and procedures. Static (using 5–10 μL droplets) and advancing contact angles (≈ 5 μL initial drop size, with ≈ 20 μL being added) can and should be measured on powders. The resulting values should be reported in combination with a description of how the surface was prepared. Receding

contact angles should not be measured on powders because the droplet will take up powder, influencing the measurement. However, roll-off angles can be measured on powders using small (5–10 μL) water droplets. In addition to performing measurements on powder, pressed tablets should be fabricated at a defined load, and the static (using 5–10 μL drops), advancing, and receding contact angles ($\approx 5\text{ }\mu\text{L}$ and $\approx 25\text{ }\mu\text{L}$ initial droplet sizes for advancing and receding angles, respectively, with $\approx 20\text{ }\mu\text{L}$ being added/withdrawn) should be measured on those tablets. The contact angles should be reported together with the applied load. The surface roughness should ideally be estimated and listed, and the contact angle measurements should be carefully interpreted based on these results. Measurements on pressed pellet disks with a low roughness give the best indication of the intrinsic wetting properties of the MOF material. However, in this context, the stability of MOFs towards mechanical pressure must be kept in mind.

4 Potential Applications of Hydrophobic MOFs and their Composites.

As discussed in the previous sections, hydrophobic MOF materials can be synthesized by various routes and have potential industrial applications in various fields. Although the industrial-scale use of hydrophobic MOFs is still far away, they have very attractive properties that make such uses quite plausible in future. This section presents some key examples that highlight recent advances in the preparation and use of hydrophobic MOFs with potential applications in hydrocarbon storage for vehicular fuel, catalysis, separation of oil spills from water.

4.1. Hydrocarbon Storage/Separation

Light hydrocarbon storage/separation is important in the chemical industry and the wider economy. Clean olefin feedstock's are necessary for the production of high-quality polymers, and their separation, currently achieved by cryo distillation, is one of the most energetically (and hence financially) expensive processes in the chemical industry. In addition, the storage of light aromatic hydrocarbons is vital for their conversion into bulk chemical products and their use as fuels. Omary et al. developed hydrophobic fluorinated MOFs (FMOF-1 and FMOF 2) that can be used to adsorb a variety of C_6 – C_8 hydrocarbons commonly found in the gasoil fraction of crude oil.^[65] The uptakes of benzene, cyclohexane, *n*-hexane, *p*-xylene and toluene by these materials were 290, 300, 190, 265, and 270 kg/m^3 , respectively (Figure 12d). These strong uptakes at low pressure indicate the presence of favorable host–guest interactions based on the confinement of the

aromatic adsorbates. It should be noted that the uptake of hydrocarbon mainly depends on the internal hydrophobic pores and the size of the channels.

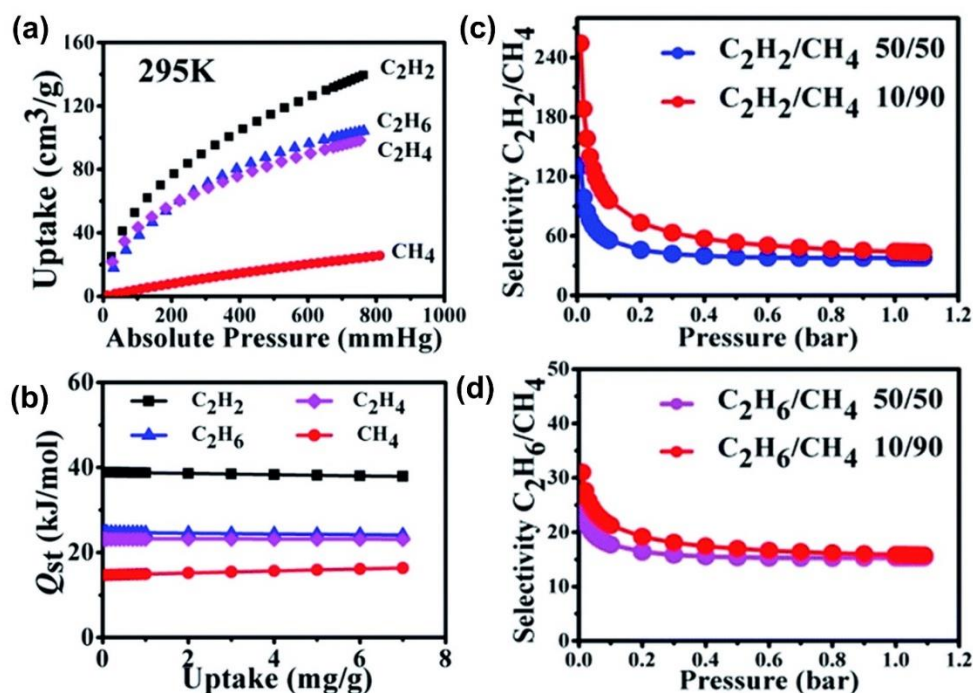


Figure 21. Hydrocarbon adsorption of **UPC-21**. The C_2H_2 , C_2H_4 , C_2H_6 and CH_4 adsorption isotherms for **UPC-21** at 295 K (b) The isosteric heat of adsorption for C_2H_2 , C_2H_4 , C_2H_6 and CH_4 . Selective adsorption of **UPC-21**. The calculations of IAST selectivities for mixtures of C_2H_2/CH_4 (e), C_2H_4/CH_4 (f), C_2H_6/CH_4 (f), C_3H_6/CH_4 (h) and C_3H_8/CH_4 (i) at 295 K. Reprinted from ref.^[197] Copyright 2014, Royal Society of Chemistry.

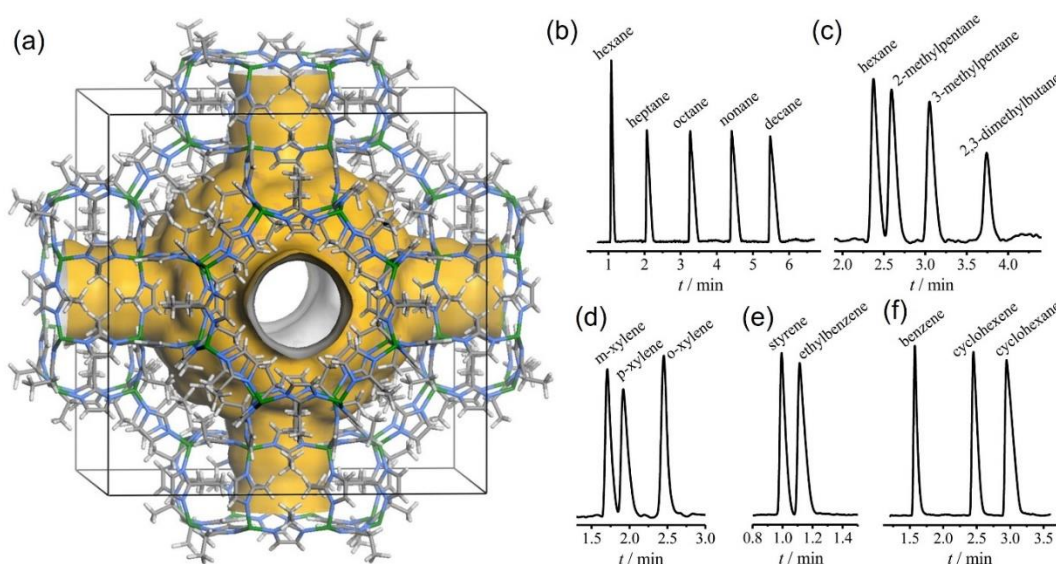


Figure 22. (a) Structure of **MAF-6** and Chromatograms on the **MAF-6**-coated capillary for GC separation of (b) linear alkanes, (c) hexane and its branched isomers, (d) xylene isomers, (e) styrene and ethylbenzene, and (f) benzene, cyclohexene, and cyclohexane. Reproduced with permission from ref.^[60] Copyright 2015, American Chemical Society.

Another linker-based hydrophobic MOF is **UPC-21**, which was successfully used for the adsorption/separation of hydrocarbons (C_1 – C_3). In addition, to its hydrophobic pores, UPC-21 is lined with open metal sites, enabling the discrimination of olefins from paraffins and short chain from long chain hydrocarbons. **UPC-21** exhibits a remarkable acetylene uptake of $139.5 \text{ cm}^3 \text{ g}^{-1}$ at 295 K (Figure 21 a). Its uptake capacities for C_2H_4 , C_2H_6 , C_3H_6 , and C_3H_8 are also fairly high at 1 bar and amount to 295 K are 98.4, 104.3, 110.1, and $103.0 \text{ cm}^3 \text{ g}^{-1}$, respectively. The isosteric heats (Q_{st}) of adsorption for C_2H_2 , C_2H_4 , and C_2H_6 are 38.8, 24.7, and 23.1 kJ mol^{-1} , respectively, indicating strong interactions between the hydrocarbons and the coordination framework (Figure 21b). The overall capacity of **UPC-21** for light hydrocarbons (C_2 – C_3) at 295 K is much higher than those of other promising MOFs such as M'MOF-3a, UTSA-67, and Cu(etz). This was attributed to the synergistic effects of its high density of open Cu(II) sites, multiple aromatic rings, and optimized pore size. On the other hand, **UPC-21** adsorbs only $25.7 \text{ cm}^3 \text{ g}^{-1}$ of CH_4 at 295 K, respectively. The calculated separation selectivities (expressed as molar ratios) for UPC-21 when exposed to equimolar mixtures of CH_4 and C_2H_2 amount to 38.1 (Figure 21 c-d). It is worth observing that **UPC-21** shows better selectivity for C_2H_2 over CH_4 at 295 K than previously reported MOFs such as MFM-130a (34.7), UTSA-36a (13.8), $Zn_4(OH)_2(1,2,4\text{-BTC})_2$ (14.7), and $Zn_5(BTA)_6(TDA)_2$ (15.5).^[197] The same group also prepared a nanoporous hydrophobic MOF $\{[In_{1.5}(\mu_3\text{-O})_{0.5}(\text{TPTA-F})(H_2O)(OH)_{0.5}] \cdot 4DMF \cdot 4.5H_2O\}$ (UPC-104) based on a fluorine-functionalized organic linker, and used it for hydrocarbon storage/separation.^[206] This framework has high stability in acidic and basic aqueous solutions and is thermally stable up to 300 °C. Moreover, UPC-104 exhibits very high H_2 ($230.8 \text{ cm}^3 \text{ g}^{-1}$, 2.06 wt% at 77 K and 1 bar), C_2H_2 ($187.0 \text{ cm}^3 \text{ g}^{-1}$ at 273 K and 1 bar), and C_3H_6/C_3H_8 adsorption capacities ($276.5 \text{ cm}^3 \text{ g}^{-1}$ and $250.4 \text{ cm}^3 \text{ g}^{-1}$ for C_3H_6 and C_3H_8 at 273 K and 1 bar).

Chen and coworkers successfully used the hydrophobic zeolite imidazole framework MAF-6 to separate alcohols and aromatic hydrocarbons from water based on its large aperture size and inherent hydrophobicity (Figure 22a).^[60, 207] In their work, the separation of hydrocarbons was achieved by gas chromatography (GC) using a quartz capillary with microcrystalline MAF-6 grafted onto its inner surface. Interestingly MAF-6 achieves good selectivity and excellent separation for diverse linear and aromatic hydrocarbons, and adsorbs large quantities of organic molecules. Interestingly, the material is able to successfully separate saturated and unsaturated molecules with similar structures (Figure 22b-f). These results indicate that stable superhydrophobic MOFs could be useful for hydrocarbon storage and separation in the future.

4.2. Oil-Water Separation:

Oil spills in oceans cause serious problems to human beings and marine life, presenting serious threats to environment and people's health. Water purification from oils, without damaging ecosystem and environmental pollution is a challenging task. The methods established for separation of oils from water, adsorptive separation holds the greatest promise due to its facile, simple and economically cheap.

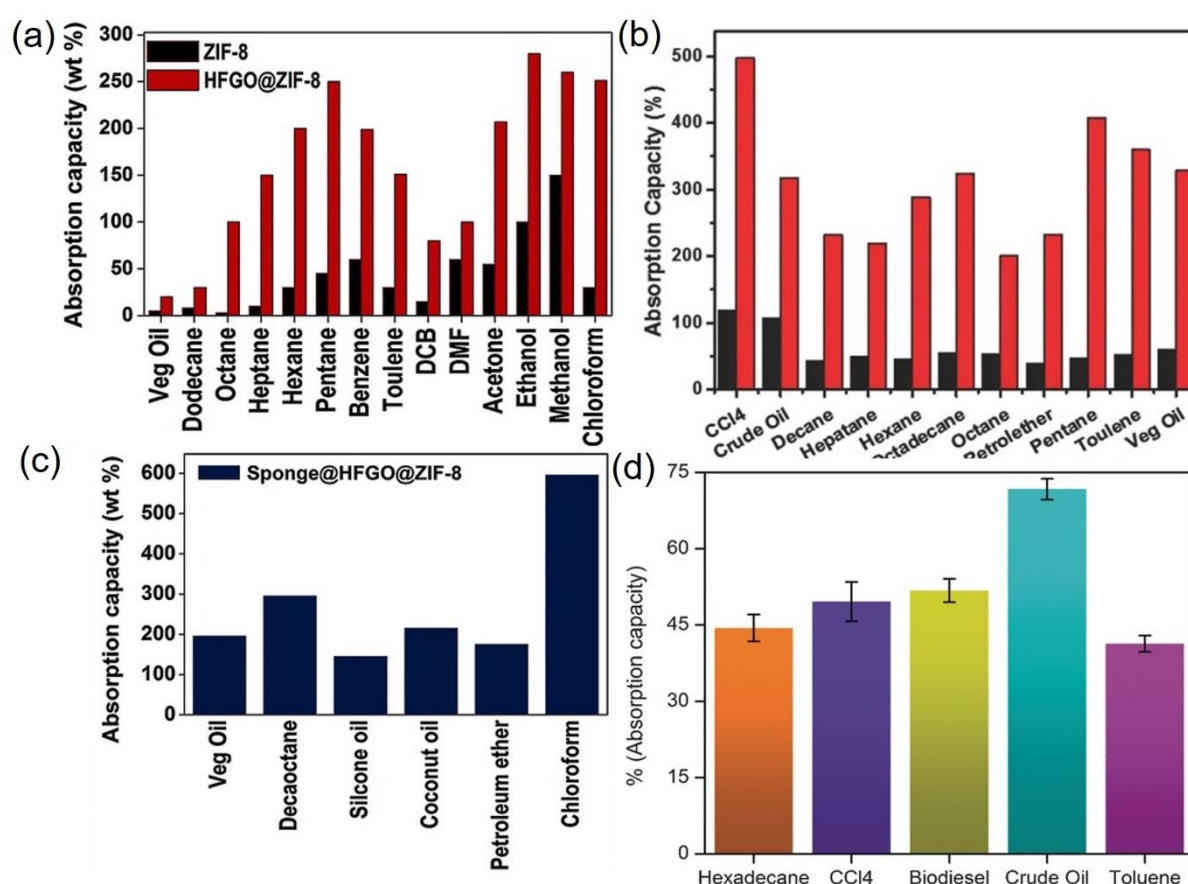


Figure 23. (a) Absorption of oils and organic solvents of hybrid **HFGO@ZIF-8** and pristine ZIF-8; (b) Oils adsorption capacity of hybrid with sponge **Sponge@HFGO@ZIF-8**; (c) Adsorption of various oils and organic solvents of **HFGO@MOG** (red bars) and **MOG** (black bars) (d) Schematic illustration of hydrophobic MOF membrane **UHMOP-100/PDMS/PP**. Bar diagram representations of the absorption capacities (e) and recycling tests (f) on **UHMOP-100/PDMS/PP**. Reproduced with permission.^[85,114,94] Copyright 2015, 2016,2017, Wiley-VCH.

A combination of hydrophobic and oleophilic graphene-based MOF composite materials was recently used successfully for oil separation: a superhydrophobic and oleophilic multi-aromatic hydrophobic MOF exhibited 100% oil separation from water and removed 99.0% of all tested

pollutants other than crude oil.²⁰⁴ Our group successfully used the hierarchical porous superhydrophobic-oleophilic composite HFGO@ZIF-8, which exhibits high adsorption of oils and various organic solvents.⁴⁶ The uptake values for the composite (which ranged from 20 to 280 wt %) were appreciably higher than those for the parent hydrophobic MOF, ZIF-8 (10–150 wt %; see Figure 23a). We also modified the composite further by incorporating it into a sponge, yielding a material designated Sponge@HFGO@ZIF-8. This sponge exhibited outstanding absorption uptake of various organic solvents and oils, with uptake values of 150–600 wt % based on the oil or solvent (Figure 23c). We also prepared meso-macro porous hydrophobic - superoleophilic fibrous materials composed of MOGs with FGO. FGO@MOG exhibits significantly higher adsorption capacity than those reported for hydrophobic MOFs in the literature, ranging from 200 to 500 wt% towards the selected oils and organic solvents (Figure 23b).⁸⁹ Another composite, UHMOF-100/PDMS/PP, features a MOF-coated polymer-based membrane and was used to adsorb several oils as crude and marine oil, biodiesel, hexadecane, carbon tetrachloride and toluene. Its adsorption capacity ($\approx 40\text{--}70$ wt %) and flux (85 ± 5 mL⁻² s⁻¹) are high and remained unchanged even after 10 cycles (Figure 23d). Banglin Chen et al. recently reported a UiO-66-coated mesh superoleophobic membrane that shows significant separation efficiency almost 99.99% oils from water.^[208] Moreover, a USTC-6@GO@sponge displays greater uptake of adsorption rates for organic solvents and oils as 1200 to 4300 wt%.^[48] Its high adsorption of oils was attributed to the microporous behaviour of USTC-6 and the sorbent's high and meso-macro porosity. Moreover, the adsorbed oils were readily separated from the USTC-6@GO@sponge because of its decent elasticity and significant mechanical stability. The authors exploited the novel characteristics of this composite to construct a simple model apparatus that enabled the successful recovery of oil from a spill in water by a straightforward 'adsorption-squeezing' process (Figure 24a). Even after prolonged cycling, the apparatus successfully recovered hexane from water (Figure 24b-c). Furthermore, the authors showed the apparatus to be capable of oil recovery even under harsh conditions (Figure 24d-i). Figure 24 J shows the recovery of diverse oils and various organic solvents viscosities of up to 100 mPa s⁻¹

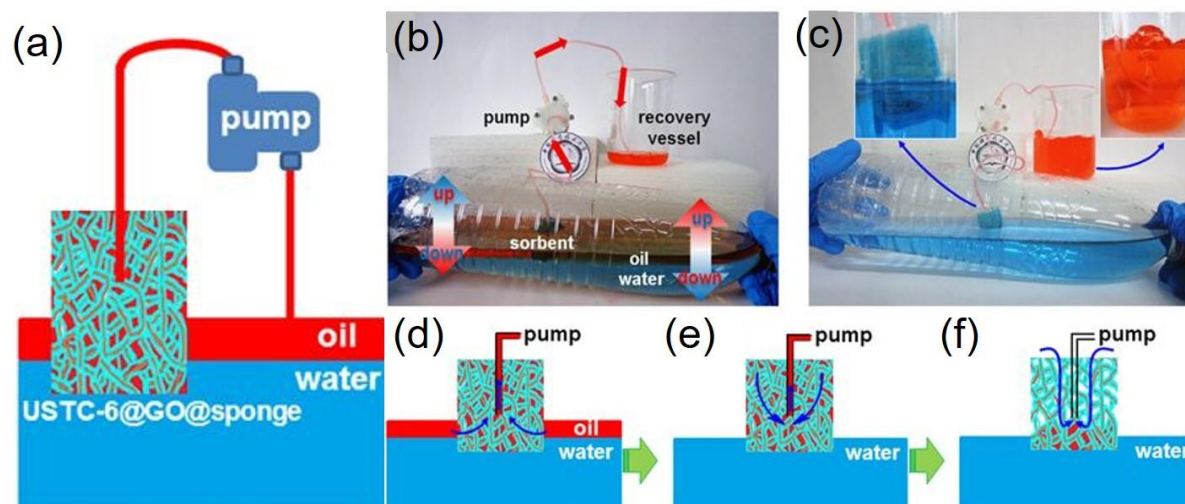


Figure 24. (a) The circulatory system used to demonstrate the consecutive oil collection capabilities of this apparatus. (b) Plot of the flux of oil (*n*-hexane) against time in the apparatus. Photographs showing (c) the apparatus continuously collecting floating oil (dyed red) on the surface of water (dyed blue) in motion, and (d) the system's status after removing all the oil from the water's surface. (f–i) An illustration of the oil recovery process: (e) aspiration of the floating oil; (g) removal of adsorbed oil above the tube nozzle; and (i) the air channel formed inside the sorbent. (f) Flow/pumping rates for oils with different viscosities. Reproduced with permission from ref.^[48] Nature 2016.

4.3. Catalysis:

The surface wettability of heterogeneous catalysts can profoundly affect their activity and selectivity by modulating their interactions with reactants and products.^[209-210] In 2016, Jiang et al. reported that hydrophobic modification can enhance catalytic performance. They performed styrene hydrogenation in a batch reaction over the pristine composite Pd/Uio-66 and a PDMS-modified hydrophobic hybrid, Pd/Uio-66@PDMS.^[81] The parental Pd/Uio-66 required 255 min to achieve complete hydrogenation (Figure 25a). However, the PDMS-coated hybrid afforded 100 % conversion within 65 min. The authors also showed that varying the thickness of the PDMS coating had no effect on the hybrid's size, electronic configuration, or (more importantly) catalytic efficiency (Figure 25b). The enhanced activity of the Pd/Uio-66@PDMS hybrid can thus be primarily ascribed to the hydrophobic responsive PDMS surface modification of the Pd surface. The composite Pd/Uio-66@PDMS catalyst was also used to hydrogenate other hydrophobic substrates as nitrobenzene and cinnamaldehyde. Additionally,

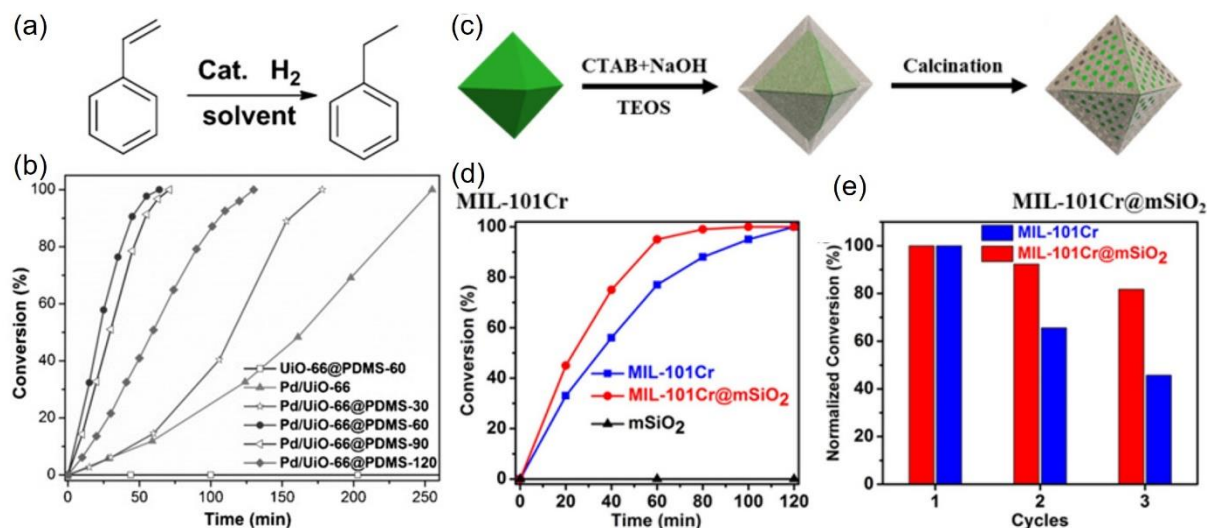


Figure 25. a) Catalytic hydrogenation of styrene over UiO-66@PDMS, Pd/UiO-66, and Pd/UiO-66@PDMS; (c) Schematic representation of the synthesis of MIL-101Cr@mSiO₂. d) Time-domain conversion of indene by MIL-101Cr, MIL-101Cr@mSiO₂, and mSiO₂. e) Comparison of the conversion for MIL-101Cr and MIL-101Cr@mSiO₂ over three reaction runs. Reproduced with permission ^[81] Wiley-VCH 2016, Reproduced with permission ^[75] American Chemical Society 2018.

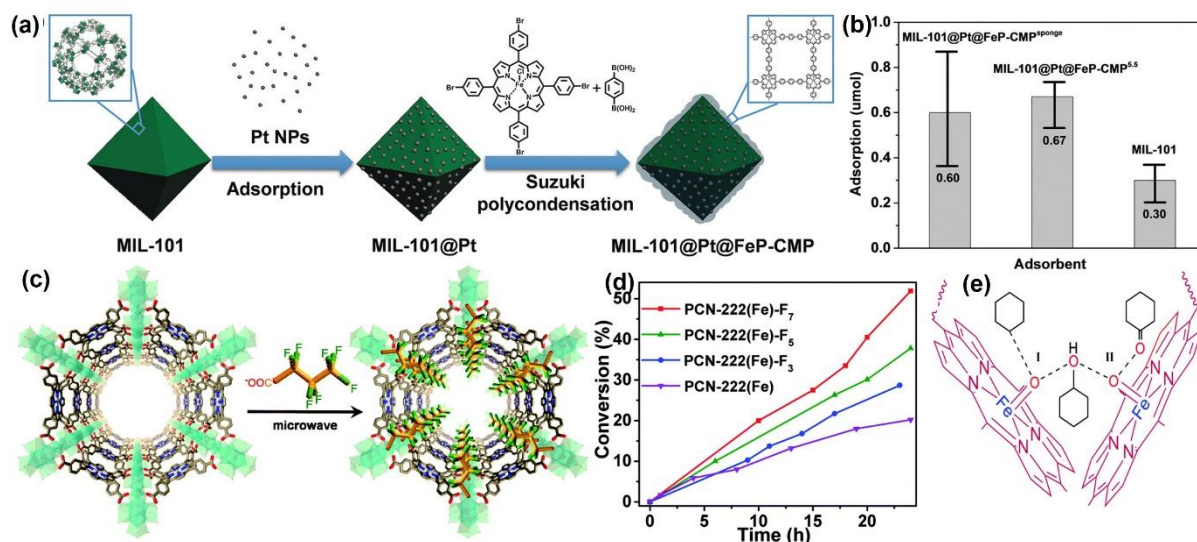


Figure 26. a) Design strategy for the synthesis of MIL-101@Pt@FeP-CMP. (b) Adsorption of cyclohexane by PCN-222(Fe) and PCN-222(Fe)-F_n (n = 3, 5 and 7) in acetonitrile over time; (c) schematic illustration of making PCN-222(Fe)-F_n from PCN-222(Fe); (d-e) Conversion-time plots for cyclohexane oxidation over PCN-222(Fe) and PCN-222(Fe)-F_n (n = 3, 5, and 7). Reproduced with permission ^[211-212] Wiley-VCH 2018 and Royal Society of Chemistry 2017.

Hydrophobic Metal–Organic Frameworks, F. Geyer et. al. ,Adv. Mater. 2019, 1900820, DOI: 10.1002/adma.201900820

Janiak and co-workers, reported that hydrophobic silica coating of MIL-101(Cr) nanoparticles improved catalytic performance and catalyst reusability for the oxidation of indene with H_2O_2 in acetonitrile (Figure 25c).^[75] MIL-101Cr@mSiO₂ shows superior catalytic activity to pristine MIL-101(Cr). Further The turnover frequency of MIL-101Cr@mSiO₂ (TOF) 95.2 mmol g⁻¹ h⁻¹) superior than MIL-101Cr (76.8 mmol g⁻¹ h⁻¹) (Figure 25d). In the same approach Hu and coworkers reported the effect of hydrophobic modification in the catalytic hydrogenation of cinnamaldehyde using iron(III) porphyrin (FeP-CMPs) to modify the surface of MIL-101@Pd to prepare MIL - 101@Pt@FeP - CMP (Figure 26a).^[211] In the same work, the authors proved that MIL - 101@Pt@FeP - CMP sponge has a greater turnover frequency (1516.1 h⁻¹), with 97.3 % selectivity for cinnamyl alcohol at 97.6 % yield (Figure 26b) . Jiang and coworkers reported hydrophobic pore surface modification of iron-porphyrinic MOF, PCN-222(Fe), and successfully exploited for catalytic performance in cyclohexane oxidation (Figure 26c-d).^[212] Remarkably, perfluorinated alkyl substituents based iron-porphyrinic MOFs significantly enhanced the MOF's activity and hydrophobicity, and improved its interactions with cyclohexane, resulting in improved conversion and selectivity for KA oil. Finally, Coskun et al. recently reported carbon nitride foam/ZIF-8 composites for separating oil spills from water and the highly competent conversion of CO₂ into chloroprene carbonate, achieving quantitative yield and excellent product selectivity.^[66]

5 Conclusions and Perspectives

This review provides a comprehensive summary of the characterization, preparation and applications of hydrophobic MOFs and their composites, highlighting state-of-the-art strategies. We discussed the basics of wetting of hydrophobic materials, followed by four strategies for preparing hydrophobic MOFs, namely (a) the use of hydrophobic ligands, (b) postsynthetic grafting of hydrophobic side chains onto reactive sites, (c) the targeted exploitation of surface corrugation to induce hydrophobicity, and (d) the preparation of hydrophobic hierarchical porous composite structures. The hydrophobic ligand strategy involves decorating the ligands of the MOF with functional groups that reduce the material's surface energy, such as perfluorinated aromatics, --CF₃ groups, or long alkyl or perfluoroalkyl chains. The use of ligands bearing perfluorinated aromatics in principle makes it possible to tune the hydrophobicity of any MOF whose ligands have one or more C-H bonds.

Hydrophobic Metal–Organic Frameworks, F. Geyer et. al. ,*Adv. Mater.* 2019, 1900820, DOI: 10.1002/adma.201900820

Moreover, this concept does not reduce the accessible pore space as much as the use of bulky sidechains. However, fluorination changes the ligands' electronic structure and it is often essential to develop new synthetic strategies to access the desired framework topologies. Furthermore, the preparation of complex perfluorinated ligands is a challenging synthetic endeavor. An alternative is to use ligands bearing long hydrophobic alkyl chains that are anchored to the ligand backbone by condensation/esterification/amidation reactions. However, as noted above, although this strategy significantly increases hydrophobicity, it also dramatically reduces accessible pore space. The use of perfluoroalkanes in this context is still very rare and, in its infancy, but the preparation of fluorinated nanocages/layers in this way is certainly an appealing idea for some applications, such as the adsorption of chlorofluorocarbons or oxygen.

Further advancement in this field will require the development of new synthetic routes and conditions that will allow perfluorinated ligands to be combined with many different SBUs in order to access the plethora of topologies that have been prepared using hydrocarbon-based linker backbones. This will also facilitate the creation of mesoporous perfluorinated MOFs, which have many practical advantages (e.g. superior mass transport through their pores).

An alternative to direct synthesis of hydrophobic MOFs is post-synthetic modification of conventional MOFs. This strategy has the advantage of being applicable to any MOF with reactive handles (e.g. open metal coordination sites or ligands bearing reactive groups). Moreover, it avoids the need for a (potentially very challenging) synthesis of fluorinated ligands as well as the synthesis of the MOF itself, and many potentially suitable reagents for substitution are commercially available. However, this strategy also has some notable drawbacks: the MOF must withstand the reaction conditions, it is only applicable to MOFs with suitable reactive sites, and the reagents must be able to penetrate into the MOF's pores.

An alternative to postsynthetic modification by chemical reactions is to coat the framework with a hydrophobic polymer. This approach seems very promising because it apparently does not affect the accessibility of the pore space. However, to date it has only been applied to MOFs with micropores; it will be very interesting to see if this process can be transferred to compounds with meso- and macropores without sacrificing porosity.

Surface Corrugation is a method that is seemingly applicable to diverse surfaces and enables selective transformation whereby the outer surface is made hydrophobic while the inner surface remains hydrophilic. At present, it can only be applied to MOFs with very specific types of ligands, but it could be a very powerful strategy if general methods for roughening the surface of (ideally) any type of MOF material were developed.

Hydrophobic Metal–Organic Frameworks, F. Geyer et. al. ,*Adv. Mater.* 2019, 1900820, DOI: 10.1002/adma.201900820

The final strategy that has been used successfully involves preparing hierarchical porous composites of metal-organic frameworks with membranes or 2D carbon materials. This strategy is very promising because it appears to be universally applicable and the resulting composites couple the beneficial properties of microporous MOFs with the desirable qualities of the other component of the composite. Most reports describing these systems have been based on MOFs that are not inherently sensitive towards water; it would be interesting to see if other more sensitive MOFs can be protected by these hierarchical structures. In general, the combination of two or more of these synthetic concepts to trigger synergistic effects would be very interesting.

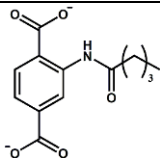
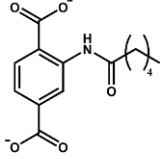
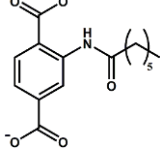
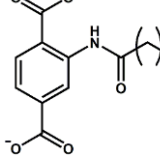
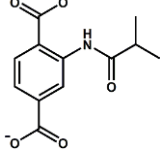
The characterization of hydrophobic MOFs poses another challenge with many pitfalls because hydrophobic MOFs often have hydrophobic pores as well as external hydrophobic surfaces. The inherent hydrophobic pores can be thoroughly characterized by measuring vapor phase adsorption isotherms for water and/or aromatic hydrocarbon. However, no standardized measurement protocol utilizing consistent pressure ranges and measurement temperatures has yet been developed. Hydrophobic pores do not usually show any appreciable water uptake, but they typically outperform traditional porous materials with respect to the uptake of benzene. The outer hydrophobic surface can be characterized by contact angle measurements. Although many advances have been made in this area, contact angle measurements still have many limitations, and there is a clear lack of standardization in this area.

This review has highlighted some critical challenges relating to contact angle measurements on the surfaces of powders, crystals, and pressed pellets before and after the evacuation of solvent molecules. While some intriguing high contact angles have been reported for various hydrophobic MOFs, contact angle measurements of supposedly hydrophobic MOFs are only rarely performed. Furthermore, it must be noted that the pressure applied during the preparation of pellets could mechanically alter some MOF structures. We also highlighted inverse gas chromatography as a promising method for surface characterization of MOFs based on the adsorption of various solvent vapor molecules.

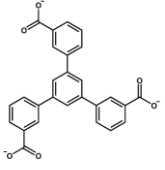
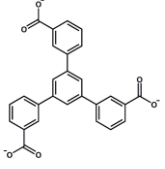
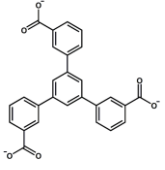
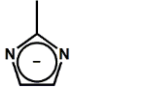
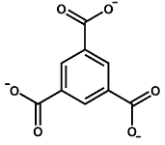
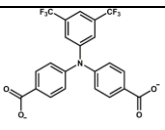
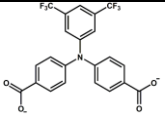
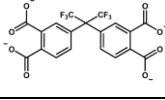
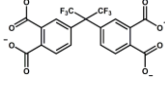
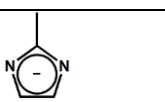
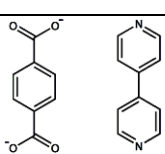
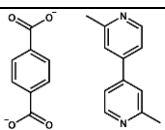
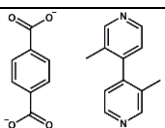
Many hydrophobic MOF/composites have potential applications in alcohol adsorption, hydrocarbon separation/storage, oil spill separation from water, and catalysis, and there are undoubtedly many other potential applications that have yet to be discovered and explored. Despite their great promise, the industrial applications of hydrophobic MOF are currently in their infancy and are limited by the chemical, physical, and mechanical stability of most reported MOF materials. Therefore, the synthesis of highly stable/hierarchical porous hydrophobic MOFs and their composites has the potential to create new opportunities, e.g. in

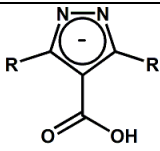
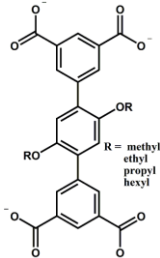
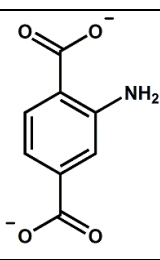
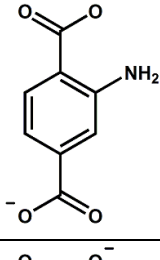
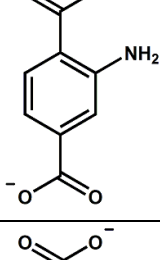
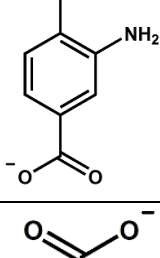
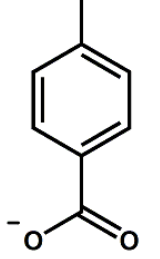
energy (storage) applications, or sensing where the enrichment of certain species from solution is important. The design and coupling of photocatalytically active and hydrophobic MOF is another interesting avenue that could enable the preparation of water-stable photocatalytic water splitting devices. Furthermore, there is the prospect of developing hydrophobic hierarchical materials that combine different functions in one material, such as MOF/2D Material/sponge hybrids for oil spill cleanup, in which a certain fraction of the crude oil is strongly adsorbed in the MOF and the other fraction in the mesopores, enabling the splitting of the oil fractions during clean up. We expect rapid development in this field and further optimization of hydrophobic MOFs and their composites for various applications, but standardized characterization methods will be needed to achieve this and to ensure comparability between different systems and their properties.

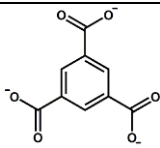
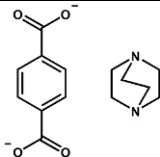
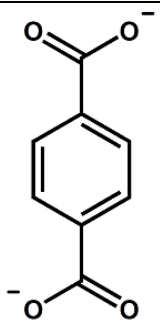
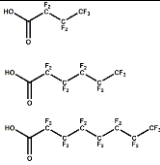
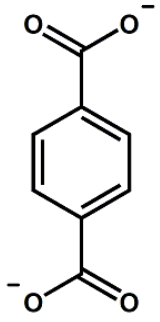
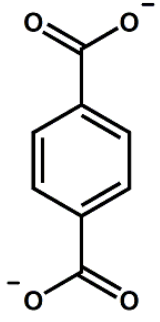
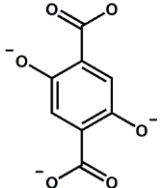
Table 2. Summary of Hydrophobic MOFs/composites and applications

Ligand Structure	Ligand Abbreviation	MOF Formula	Responsible Hydrophobicity	Contact Angle [degree]	Application	Ref
	bdc ²⁻ -AM4	IRMOF-3-AM4 Zn ₄ O(bdc-AM4) ₃	Alkyl chain (C4)	116 ± 6	-	[74]
	bdc ²⁻ -AM5	IRMOF-3-AM5 Zn ₄ O(bdc-AM5) ₃	Alkyl chain (C5)	119 ± 10		[74]
	bdc ²⁻ -AM6	IRMOF-3-AM6 Zn ₄ O(bdc-AM6) ₃	Alkyl chain (C6)	124 ± 8		[74]
	bdc ²⁻ -AM15	IRMOF-3-AM15 Zn ₄ O(bdc-AM15) ₃	Alkyl chain (C15)	123 ± 5		[74]
	bdc ²⁻ -AMiPr	IRMOF-3-AMiPr Zn ₄ O(bdc-AMiPr) ₃	Alkyl chain	125 ± 12		[74]


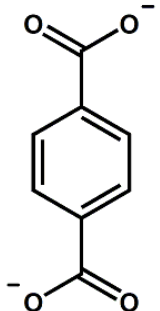
	bdc ²⁻ -AMiBu	IRMOF-3-AMiBu Zn ₄ O(bdc-AMiBu) ₃	Alkyl chain	105 ± 11		[74]
	bdc ²⁻ -AM4	MIL-53(Al)-AM4 Al(OH)(bdc-AM4)	Alkyl chain (C4)	>150		[74]
	bdc ²⁻ -AM6	MIL-53(Al)-AM6 Al(OH)(bdc-AM6)	Alkyl chain (C6)	>150		[74]
	Tz ⁻	FMOF-1 Ag ₄ Tz ₆	CF ₃ functionalized organic linker	-	Hydrocarbon (C6-C8) Storage	[65]
	Tz ⁻	FMOF-2 Ag ₃ Tz ₄	CF ₃ functionalized organic linker	-	Hydrocarbon (C6-C8) Storage	[65]
	OFBPDC ²⁻	MOFF-1 Cu ₂ (OFBPDC) ₂ (MeOH) ₂	perfluorinated aromatic ring	108 ± 2	-	[89]
	OFBPDC ²⁻	MOFF-2 Cu ₂ (OFBPDC) ₂ (DABCO)	perfluorinated aromatics	151 ± 1	-	[89]
	PFBPTZ ²⁻	MOFF-3 Cu(PFBPTZ)(H ₂ O)	perfluorinated aromatics	135 ± 2	-	[89]
	OPE-C ₁₈ ²⁻	NMOF-1 Zn(OPE-C ₁₈)(H ₂ O) ₂	Alkyl chain	160-162	Self-cleaning	[151]
	PEIP ⁴⁻	UPC-21 Cu ₃ (PEIP) _{1.5} (H ₂ O) ₃	Multiple-aromatic rings	145 ± 1	Hydrocarbon separation, Oil spills separation from water	[197]
	TPTA-F ³⁻	UPC-104 [In _{1.5} (μ ₃ -O) _{0.5} (TPTA-F)(H ₂ O)(OH) _{0.5}	F-functionalized organic linker	-	C1-C4 hydrocarbon storage/separation	[206]
	eim ⁻	MAF-6 RHO-Zn(eim) ₂	Internal pore and external crystal surfaces	143 ± 1	6–C10 hydrocarbons	[60]
	eim ⁻	MAF-5 ANA-Zn(eim) ₂	0	0	0	[60]
	mIm ⁻	MAF-4/ZIF-8 Zn(mIm) ₂	0	0	0	[60]

	BTMB ³⁻	PESD-1 Zn ₄ (μ ₃ -OH) ₂ (BTMB) ₂	Surface corrugation	150	Aromatic hydrocarbon storage	[53]
	BTMB ³⁻	PESD-2 Zn ₂ Co ₂ (μ ₃ -OH) ₂ (BTMB) ₂	Surface corrugation	159	Aromatic Hydrocarbon Storage Oil spill clean up from sea water	[198]
	BTMB ³⁻	PESD-3 Zn ₂ Ni ₂ (μ ₃ -OH) ₂ (BTMB) ₂		161	Aromatic Hydrocarbon storage Oil spil clean up from seawater	[198]
	mIm ⁻	HFGO@ZIF-8	Highly Fluorinated graphene oxide	162	Oil-water separation , self-cleaning	[114]
	BTC ³⁻	FGO@ALMOG	Highly Fluorinated graphene oxide	150	Oil-water Separation	[85]
	BTFPADB ²⁻	UHMOF-100 Cu ₂ (BTFPADB) ₂	CF ₃ functionalized organic linker	176	Aromatic Hydrocarbon storage	[94]
	BTFPADB ²⁻	UHMOF-100/PDMS/PP Cu ₂ (BTFPADB) ₂	CF ₃ functionalized organic linker	135	Oil-water separation	[94]
	HFPD ⁴⁻	USTC-6 Cu ₂ (HFPD)	CF ₃ functionalized organic linker	-	Aromatic hydrocarbon storage	[48]
	HFPD ⁴⁻	USTC-6@GO@sponge	CF ₃ functionalized organic linker	128	Oil-spills separation from water and recovery under harsh conditions	[48]
	mIm	SIM-2(C ₁₂) SIM-1 isostructural with ZIF-8	post-synthetic modification with long alkyl chains		Catalysis Knoevenagel condensation	[55]
	BDC, BIPY	MOF-508 Zn ₂ (bdc) ₂ (bipy)			Toulene adsorption	[93]
	BDC, 2,2'-DM-BIPY	SCUTC-18	Linker Functionalization		Toulene adsorption	[93]
	BDC, 3,3'-DM-BIPY	SCUTC-19	Linker Functionalization		Toulene adsorption	[93]

	3,5-dimethyl-4-carboxypyrazolato	$\text{Zn}_4\text{O}(\text{dmcapz})_3$	Linker functionalization		Adsorption of small organic probe molecules	[45]
	TPTC-OR ⁴⁻	$\text{Cu}_2(\text{TPTC-OR})$	Linker Functionalization		Tuning moisture and thermal stability of MOFs	[92]
	$\text{NH}_2\text{-BDC}^{2-}$	UiO-66- $\text{NH}_2\text{@MON-1}$ $\text{Zr}_6\text{O}_4(\text{OH})_4(\text{NH}_2\text{-BDC})_{12}$	Post-synthetic encapsulation in MON (microporous organic framework)	121	Adsorption organic compounds	[72]
	$\text{NH}_2\text{-BDC}^{2-}$	UiO-66- $\text{NH}_2\text{@MON-2}$ $\text{Zr}_6\text{O}_4(\text{OH})_4(\text{NH}_2\text{-BDC})_{12}$	Post-synthetic encapsulation in MON (microporous organic framework)	139	Adsorption organic compounds	[72]
	$\text{NH}_2\text{-BDC}^{2-}$	UiO-66- $\text{NH}_2\text{@MON-3}$ $\text{Zr}_6\text{O}_4(\text{OH})_4(\text{NH}_2\text{-BDC})_{12}$	Post-synthetic encapsulation in MON (microporous organic framework)	145	Adsorption organic compounds	[72]
	$\text{NH}_2\text{-BDC}^{2-}$	UiO-66- $\text{NH}_2\text{@MON-4}$ $\text{Zr}_6\text{O}_4(\text{OH})_4(\text{NH}_2\text{-BDC})_{12}$	Post-synthetic encapsulation in MON (microporous organic framework)	124	Adsorption organic compounds	[72]
	BDC^{2-}	MOF-5 $\text{Zn}_4\text{O}(\text{BDC})_3$	PDMS Coating	128	Gas sorption catalysis	[62]

	BTC ³⁻	HKUST-1 Cu ₃ (BTC) ₂	PDMS Coating	130	Gas sorption catalysis	[62]
	BDC ²⁻ DABCO	Zn ₂ (BDC) ₂ (DABCO)	PDMS Coating	130	Gas sorption catalysis	[62]
	BDC ²⁻	UiO-66/Pd/PDMS Zr ₆ O ₄ (OH) ₄ (BDC) ₁₂	PDMS Coating	140	hydrogenation of styrene catalysis	[81]
	TCPP ⁴⁻	PCN-222(Fe)-F ₇ Zr ₆ (OH) ₄ (Fe-TCPP) ₄	Post synthetic modification with different perfluorinated acids	135	catalysis	[212]
	BDC ²⁻	MIL-101 (Cr) Cr ₃ O(OH)(H ₂ O) ₂ (BDC) ₃	Modification of MOF surface with silica		catalysis	[75]
		MIL-101@Pt@FeP-CMP Cr ₃ O(OH)(H ₂ O) ₂ (BDC) ₃	Surface modification with conjugated micro- and mesoporous polymer	123	catalysis	[75]
	DOBDC ⁴⁻	Ni ₂ DOBDC	incorporating hydrophobic moieties on the external surface of the MOFs <i>via</i> physical adsorption		Moisture stability	[67]

		MIL-101(Cr) $\text{Cr}_3\text{O}(\text{OH})(\text{H}_2\text{O})_2(\text{BDC})_3$	incorporating hydrophobic moieties on the external surface of the MOFs via physical adsorption		Moisture stability	[67]
		HKUST-1 $\text{Cu}_3(\text{BTC})_2$	PVDF Coating		Ammonia Adsorption	[56]
		MOF-5 $\text{Zn}_4\text{O}(\text{BDC})_3$	Growing polymers inside the pores (polynaphthylene)		Carbon capture	[78]
	tdc = 2,5-thiophenedicarboxylate	DUT-67-Pfba	Post synthetic modification with different perfluorinated acids	119	Stability enhancement	[83]
	BAPy = 1,3,6,8-tetrakis(perfluorinated benzoate)pyrene	Pd@Fn-NU-1000	Post synthetic modification with different perfluorinated acids		catalysis	[97]
	1,2-bis[1,2-dicarboxyphenyl]-1,2-dodecaborane (oCB-L)	$[\text{Zn}_4(\mu_4\text{-bdc})_2(\mu_2\text{-oCB-L})_2(\mu_3\text{-O})_2(\text{DMF})_2] \cdot 4\text{DMF}$	hydrophobic carborane-based linker	140	-	[90]
	2,4,6-tri(pyridin-4-yl)-1,3,5-triazine	MFOF-1	fluoride- and sulfate-bridged cubane-type tetranuclear cobalt clusters		Aromatic vapor adsorption	[68]
	2-methylimidazole	ZIF-8/Carbon Nitride Foam	Carbon nitride foam	139	Oil-water separation Chemical fixation of CO_2	[66]
	asp^{2-}	$\text{Ni}_2(\text{L-aspartate})_2\text{bipy@PDMS}$	PDMS coating	130	high flux of H_2O and acceptable separation factor	[99]

	Benzimidazole	ZIF-7	Linker functionalization	151	Oil spills separation of water	[77]
	BDC	UiO-66/mesh membranes	Mesh membranes		Oil-water separation	[208]

Bio:



Jayaramulu Kolleboyina was born in Vijayawada, INDIA. He obtained his masters at Banaras Hindu University and conducted PhD studies in Materials Chemistry at the Jawaharlal Nehru Centre for Scientific Research, Bangalore, graduating in 2014. After his PhD, he worked with Prof. Dr. CNR Rao, ICMS Bangalore, and at ICN2, Barcelona, Spain with Prof. Daniel Maspocho. He has been a postdoctoral fellow with Prof. Roland A Fischer with Alexander von Humboldt postdoctoral Fellowship (2015-2016) at Ruhr-University Bochum. He is currently working as a senior researcher at Technical University Munich, Germany and the Regional Centre of Advanced Technologies and Materials, Czech Republic. His research focuses on the synthesis, design, and characterization of hybrid porous materials including metal-organic frameworks, graphene derivatives, and new 2D materials for various environmental (water purification, gas storage/separation) and energy-related (water splitting and batteries) applications.



Florian Geyer studied chemistry in Mainz, Germany and Ithaca, New York. He is currently a PostDoc at the Max Planck Institute for Polymer Research where he also obtained his PhD. In 2018, he was a visiting scholar at the Osaka Institute of Technology. His research interests focus on the fundamentals of wetting, the fabrication of superhydrophobic and superomniphobic surfaces, and their applications as gas exchange membranes, self-cleaning, and anti-biofouling surfaces.



Andreas Schneemann grew up in Sprockhövel, Germany. He obtained his M.Sc. and Ph.D. at the Ruhr University Bochum under the guidance of Prof. Roland A. Fischer, working on metal–organic frameworks. He was then a visiting scholar in the laboratories of Ian A. Fallis (Cardiff University), Seth M. Cohen (University of California, San Diego), and Shin-ichiro Noro (Hokkaido University). After a short stay as a scientific staff member at Technical University Munich, he joined the group of Mark D. Allendorf at Sandia National Laboratories in Livermore, California, on a German Research Foundation (Deutsche Forschungsgemeinschaft) Fellowship.

Hydrophobic Metal–Organic Frameworks, F. Geyer et. al. ,Adv. Mater. 2019, 1900820, DOI: 10.1002/adma.201900820

His current research interests revolve around hydrogen storage materials, particularly metal hydrides confined in porous matrices.



Štěpán Kment received his PhD in solid state physics and photoelectrochemistry in 2010 from the Czech Technical University in Prague, Czech Republic. He then spent a year as a postdoctoral research fellow at the Department of Electrical Engineering, University of Nebraska – Lincoln, Lincoln, NE, USA. Since 2011, he has been working at the Regional Centre of Advanced Technologies and Materials of Palacký University, Olomouc, Czech Republic as a Senior Researcher and since 2017 as the Photoelectrochemistry group leader. His research is focused on the development of new materials and nanostructures for renewable energy applications such as PEC water splitting, CO₂ reduction, and PEC solar cells.



Michal Otyepka (1975) received his Ph.D. degree in Physical Chemistry at the Palacký University, Olomouc, Czech Republic (2004). He is currently head of the Department of Physical Chemistry at the Palacký University, Olomouc, and vice-director of the Regional Centre of Advanced Technologies and Materials, Palacký University, Olomouc. His research is focused on the design, properties, chemistry and applications of new 2D materials, graphene derivatives, non-covalent interactions with nanomaterials, surface properties of (nano)materials, and modeling of complex molecular systems and nanomaterials.



Radek Zboril received his PhD. degree at the Palacký University in Olomouc, Czech Republic. After his doctoral studies, he underwent several foreign stays at universities around the world in locations such as Tokyo, Delaware, and Johannesburg. Currently, he is a professor at the Department of Physical Chemistry and a General Director of the Regional Centre of Advanced Technologies and Materials at the Palacký University in Olomouc, Czech Republic. His research interests focus on nanomaterial research including iron- and iron oxide-based nanoparticles, silver nanoparticles, carbon nanostructures, and magnetic nanoparticles, their synthesis, physicochemical characterization, and applications in catalysis, water treatment, antimicrobial treatment, medicine, and biotechnology.



Doris Vollmer studied physics at the University of Bielefeld, Zürich and Utrecht. After her PhD on microemulsions she moved to Mainz and started working on phase transitions in microemulsions and their dynamics. In Dec. 2002 she joined the group of Hans-Jürgen Butt at the Max Planck Institute for Polymer Research and was appointed as a professor in the physics department of the University of Mainz in 2015. Since 2009 she is investigating the wetting behavior of droplets on surfaces, focusing on superhydrophobicity and lubricant impregnated surfaces



Roland A. Fischer received his Dr. rer. nat. (1989) and Habilitation (1995) from Technical University Munich (TUM). He was Associate Professor at Heidelberg University (1996-1997) and Full Professor for Inorganic Chemistry at Ruhr-University Bochum (1997-2015). In 2016 he returned to TUM and took the Chair of Inorganic and Metal-Organic Chemistry. He has been elected Vice President of the Deutsche Forschungsgemeinschaft (DFG) in 2016. Since 2017 he is Director of TUM Catalysis research Centre. His research focuses on main group 13/transition metal compounds and clusters, precursors for metal-organic chemical vapor deposition (MOCVD) and the materials chemistry of metal-organic frameworks (MOFs) in the context of catalysis and energy materials.

List of abbreviations

MOF	Metal-organic framework
2meIM	2-methylimidazole
AFM	Atomic force microscopy
BDC	benzene dicarboxylate
BET	Brunauer-Emmet-Teller
BTC	Benzenetricarboxylate
BTMB	1,3,5-tris(3-carboxyphenyl)benzene
CAH	Contact Angle hysteresis
DABCO	1,4-diazabicyclo[2.2.2]octane
DOBDC	2,5-dioxido-1,4-benzenedicarboxylate
eIM	ethyl imidazole
F	Fluorine
FGO	Fluorinated graphene oxide
FMOF	Fluorous metal–organic framework

GO	Graphene oxide
H ₂ BTFPADB	(4,4'-{[3,5-bis(trifluoromethyl)phenyl] azanediyldibenzoic acid
H ₂ OFBPDC	2,2',3,3',5,5',6,6'-Octafluorobiphenyl-4,4'-dicarboxylic acid
H ₂ PFBPTZ	5,5'-(Perfluorobiphenyl-4,4'-diyl)bis(1H-tetrazole
H ₃ TPTA-F	2'-fluoro-[1,1':3',1''-terphenyl]-4,4'',5'-tricarboxylic acid
H ₄ HFPD	4, 4'-(hexafluoroiso propylidene) diphthalic acid
HKUST	Hong Kong university of science and technology
iGC	Inverse gas chromatography
IRMOF	Isorecticular metal-organic framework
MAF	Metal-azolate framework
MIL	Materiaux de institute Lavoisier
NH ₂ -BDC	2-amino-1,4-benzenedicarboxylate
NLDFT	Non-Localized Density Functional Theory
NMOF	Nanoscale metal-organic framework
OPE	oligo-(<i>p</i> -phenyleneethynylene)dicarboxylate
OWRK	Owens-Wendt-Rabel-Kaelble
PCN	Porous coordination network
PCN	Porous Coordination Network
PDMS	Polydimethylsiloxane
PEIP	4,4'-(Pentiptycene-6,13-diyl-bis(ethyne-2,1-diyl)isophthalic acid)
PESD	Polymer with external surface design
PS	Post synthetic
PSM	Post synthetic modification
PXRD	Powder crystal x-ray diffraction
RT	Room Temperature
SEM	Scanning electron microscopy
SU	Silica Coated
SXRD	Single crystal x-ray diffraction
TEM	Transmission electron microscopy
TOF	turnover frequency
TZ	3,5-bis(trifluoromethyl)-1,2,4-triazolate
UHMOF	Ultrahydrophobic metal-organic framework
Uio	Universiteit Oslo
UPC	Highly hydrophobic porous metal–organic framework
USTC	University of Science and Technology of China
UTSA	University of Texas at San Antonio
UV/Vis	Ultraviolet / visible light
vOCG	van Oss, Chaudhury and Good
XPS	X-ray photoelectron spectroscopy
XRD	X-ray diffraction
ZIF	Zeolitic imidazolate framework

Acknowledgments and notes

K.J.R and F.G contributed equally contributed to this review. A.S. gratefully acknowledges the German Research Foundation (Deutsche Forschungsgemeinschaft) for a Postdoctoral Fellowship (SCHN 1539/1-1). The authors also gratefully acknowledge support from the Ministry of Education, Youth and Sports of the Czech Republic (LO1305) and the assistance provided by the Research Infrastructure NanoEnviCz, supported by the Ministry of Education, Youth and Sports of the Czech Republic under Project No. LM2015073. The authors also gratefully acknowledge support the Operational Programme Research, Development and Education—European Regional Development Fund, projects no. CZ.02.1.01/0.0/0.0/15_003/0000416 and CZ.02.1.01/0.0/0.0/16_019/0000754 of the Ministry of Education, Youth and Sports of the Czech Republic.

References

- [1] H. Furukawa, K. E. Cordova, M. O’Keeffe, O. M. Yaghi, *Science* **2013**, *341*, 1230444.
- [2] M. O’Keeffe, O. M. Yaghi, *Chem.Rev.* **2012**, *112*, 675.
- [3] H. Furukawa, U. Müller, O. M. Yaghi, *Angew.Chem.Int.Ed.* **2015**, *54*, 3417.
- [4] J. L. C. Rowsell, O. M. Yaghi, *Micropor. Mesopor. Mat.* **2004**, *73*, 3.
- [5] O. M. Yaghi, *J.Am.Chem.Soc.* **2016**, *138*, 15507.
- [6] M. J. Kalmutzki, N. Hanikel, O. M. Yaghi, *Sci.Adv.* **2018**, *4*.
- [7] T. M. Osborn Popp, O. M. Yaghi, *Acc.Chem.Res.* **2017**, *50*, 532.
- [8] B. Rungtaweeworant, C. S. Diercks, M. J. Kalmutzki, O. M. Yaghi, *Faraday Discuss.* **2017**, *201*, 9.
- [9] A. Schoedel, M. Li, D. Li, M. O’Keeffe, O. M. Yaghi, *Chem.Rev.* **2016**, *116*, 12466.
- [10] M. Li, D. Li, M. O’Keeffe, O. M. Yaghi, *Chem.Rev.* **2014**, *114*, 1343.
- [11] Y. Ikezoe, G. Washino, T. Uemura, S. Kitagawa, H. Matsui, *Nature Mat.* **2012**, *11*, 1081.
- [12] S. Kitagawa, R. Kitaura, S. I. Noro, *Angew.Chem.Int.Ed.* **2004**, *43*, 2334.
- [13] T. Kitao, Y. Zhang, S. Kitagawa, B. Wang, T. Uemura, *Chem.Soc.Rev.* **2017**, *46*, 3108.
- [14] S. Horike, S. Shimomura, S. Kitagawa, *Nature Chem.* **2009**, *1*, 695.
- [15] S. Dissegna, K. Epp, W. R. Heinz, G. Kieslich, R. A. Fischer, *Adv.Mater.* **2018**, *30*.
- [16] Y. H. Hu, L. Zhang, *Adv.Mater.* **2010**, *22*, E117.
- [17] L. Jiao, Y. Wang, H. L. Jiang, Q. Xu, *Adv.Mater.* **2018**, *30*.
- [18] B. Li, H. M. Wen, Y. Cui, W. Zhou, G. Qian, B. Chen, *Adv.Mater.* **2016**, *28*, 8819.
- [19] S. T. Meek, J. A. Greathouse, M. D. Allendorf, *Adv.Mater.* **2011**, *23*, 249.
- [20] X. Zhao, Y. Wang, D. S. Li, X. Bu, P. Feng, *Adv.Mater.* **2018**, *30*.
- [21] Z. Song, N. Cheng, A. Lushington, X. Sun, *Catal.* **2016**, *6*.
- [22] S. Sundriyal, H. Kaur, S. K. Bhardwaj, S. Mishra, K. H. Kim, A. Deep, *Coord.Chem.Rev.* **2018**, *369*, 15.
- [23] H. Vardhan, M. Yusubov, F. Verpoort, *Coord.Chem.Rev.* **2016**, *306*, 171.
- [24] K. Meyer, M. Ranocchiari, J. A. Van Bokhoven, *Energy Environ. Sci.* **2015**, *8*, 1923.
- [25] Z. Lei, C. Gao, L. Chen, Y. He, W. Ma, Z. Lin, *J.Mater.Chem.B* **2018**, *6*, 1581.
- [26] T. D. Bennett, A. K. Cheetham, A. H. Fuchs, F. X. Coudert, *Nat Chem* **2016**, *9*, 11.

Hydrophobic Metal–Organic Frameworks, F. Geyer et. al. ,*Adv. Mater.* 2019, 1900820, DOI: 10.1002/adma.201900820

- [27] M. Eddaoudi, *Nature Mat.* **2007**, 6, 718.
- [28] T. Hasell, A. I. Cooper, *Nature Rev. Mater.* **2016**, 1.
- [29] S. Yuan, L. Feng, K. Wang, J. Pang, M. Bosch, C. Lollar, Y. Sun, J. Qin, X. Yang, P. Zhang, Q. Wang, L. Zou, Y. Zhang, L. Zhang, Y. Fang, J. Li, H. C. Zhou, *Adv.Mater.* **2018**, 30.
- [30] C. Wang, X. Liu, N. Keser Demir, J. P. Chen, K. Li, *Chemical Society Reviews* **2016**, 45, 5107.
- [31] N. Zhao, P. Li, X. Mu, C. Liu, F. Sun, G. Zhu, *Faraday Discuss.* **2017**, 201, 63.
- [32] Y. J. Lee, Y. J. Chang, D. J. Lee, J. P. Hsu, *J.Taiwan. Inst .Chem.E* **2018**, 93, 176.
- [33] Z. Zhang, X. Y. Liu, *Chem.Soc.Rev.* **2018**, 47, 7116.
- [34] D. Ahmad, I. van den Boogaert, J. Miller, R. Presswell, H. Jouhara, *Energy Sources, Part A: Recovery, Utilization and Environmental Effects* **2018**, 40, 2686.
- [35] A. G. Papathanasiou, *Curr. Opin. Colloid Interface Sci.* **2018**, 36, 70.
- [36] Y. Lin, H. Chen, G. Wang, A. Liu, *Coatings* **2018**, 8.
- [37] S. K. Sethi, G. Manik, *Polymer - Plastics Technology and Engineering* **2018**, 57, 1932.
- [38] X. Jing, Z. Guo, *J.Mater.Chem.A* **2018**, 6, 16731.
- [39] K. Ellinas, A. Tserepi, E. Gogolides, *Adv. Colloid Interface Sci.* **2017**, 250, 132.
- [40] C. Zhou, Z. Xin, *Progress in Chemistry* **2018**, 30, 112.
- [41] W. Li, J. Yong, Q. Yang, F. Chen, Y. Fang, X. Hou, *Wuli Huaxue Xuebao/ Acta Physico - Chimica Sinica* **2018**, 34, 456.
- [42] Z. Qian, Z. Wu, S. Wang, H. Zhang, H. Liu, X. Ye, Q. Li, *Cailiao Daobao/Materials Review* **2018**, 32, 102.
- [43] P. Z. Moghadam, J. F. Ivy, R. K. Arvapally, A. M. dos Santos, J. C. Pearson, L. Zhang, E. Tylianakis, P. Ghosh, I. W. H. Oswald, U. Kaipa, X. Wang, A. K. Wilson, R. Q. Snurr, M. A. Omary, *Chem.Sci.* **2017**, 8, 3989.
- [44] T.-H. Chen, W. Kaveevivitchai, A. J. Jacobson, O. Š. Miljanić, *Chem. Commun.* **2015**, 51, 14096.
- [45] A. Bétard, S. Wannapaiboon, R. A. Fischer, *Chem. Commun.* **2012**, 48, 10493.
- [46] R. Navarro Amador, L. Cirre, M. Carboni, D. Meyer, *J. Environ.Managment* **2018**, 214, 17.
- [47] C. Montoro, F. Linares, E. Quartapelle Procopio, I. Senkovska, S. Kaskel, S. Galli, N. Masciocchi, E. Barea, J. A. R. Navarro, *J.Am.Chem.Soc.* **2011**, 133, 11888.
- [48] Z.-R. Jiang, J. Ge, Y.-X. Zhou, Z. U. Wang, D. Chen, S.-H. Yu, H.-L. Jiang, *Npg Asia Materials* **2016**, 8, e253.
- [49] M. Mazaj, T. Čendak, G. Buscarino, M. Todaro, N. Zabukovec Logar, *J.Mater.Chem.A* **2017**, 5, 22305.
- [50] Y. Chen, B. Wang, X. Wang, L.-H. Xie, J. Li, Y. Xie, J.-R. Li, *ACS App.Mater.Interfaces* **2017**, 9, 27027.
- [51] K. P. Rao, Y. K. Devi, J. Suryachandram, R. P. Rao, J. N. Behera, *Inorg.Chem.* **2017**, 56, 11184.
- [52] H. J. Jeon, R. Matsuda, P. Kanoo, H. Kajiro, L. Li, H. Sato, Y. Zheng, S. Kitagawa, *Chem. Commun.* **2014**, 50, 10861.
- [53] K. P. Rao, M. Higuchi, K. Sumida, S. Furukawa, J. Duan, S. Kitagawa, *Angew.Chem.Int.Ed.* **2014**, 53, 8225.
- [54] H. Jasuja, K. S. Walton, *Dalton Trans.* **2013**, 42, 15421.
- [55] J. Canivet, S. Aguado, C. Daniel, D. Farrusseng, *ChemCatChem* **2011**, 3, 675.
- [56] J. B. DeCoste, J. M. S. Denny, G. W. Peterson, J. J. Mahle, S. M. Cohen, *Chem.Sci.* **2016**, 7, 2711.

- [57] H. Li, W. Shi, K. Zhao, H. Li, Y. Bing, P. Cheng, *Inorg.Chem.* **2012**, 51, 9200.
- [58] T. Wu, L. Shen, M. Luebbbers, C. Hu, Q. Chen, Z. Ni, R. I. Masel, *Chem. Commun.* **2010**, 46, 6120.
- [59] T. Wittmann, R. Siegel, N. Reimer, W. Milius, N. Stock, J. Senker, *Chem. Eur. J.* **2014**, 21, 314.
- [60] C.-T. He, L. Jiang, Z.-M. Ye, R. Krishna, Z.-S. Zhong, P.-Q. Liao, J. Xu, G. Ouyang, J.-P. Zhang, X.-M. Chen, *J.Am.Chem.Soc.* **2015**, 137, 7217.
- [61] J. Kou, L.-B. Sun, *ACS App.Mater.Interfaces* **2018**, 10, 12051.
- [62] W. Zhang, Y. Hu, J. Ge, H.-L. Jiang, S.-H. Yu, *J.Am.Chem.Soc.* **2014**, 136, 16978.
- [63] G. Wen, Z. Guo, *Colloids and Surfaces A: Physicochemical and Engineering Aspects* **2018**, 541, 58.
- [64] H. Li, M. R. Hill, R. Huang, C. Doblin, S. Lim, A. J. Hill, R. Babarao, P. Falcaro, *Chem. Commun.* **2016**, 52, 5973.
- [65] C. Yang, U. Kaipa, Q. Z. Mather, X. Wang, V. Nesterov, A. F. Venero, M. A. Omary, *J.Am.Chem.Soc.* **2011**, 133, 18094.
- [66] D. Kim, D. W. Kim, O. Buyukcakir, M.-K. Kim, K. Polychronopoulou, A. Coskun, *Adv. Funct. Mater.* **2017**, 27, 1700706.
- [67] C. A. Fernandez, S. K. Nune, H. V. Annapureddy, L. X. Dang, B. P. McGrail, F. Zheng, E. Polikarpov, D. L. King, C. Freeman, K. P. Brooks, *Dalton Trans.* **2015**, 44, 13490.
- [68] L. Zhang, W. Yang, X.-Y. Wu, C.-Z. Lu, W.-Z. Chen, *Chem. Eur. J.* **2016**, 22, 11283.
- [69] Y. Chen, B. Wang, X. Wang, L. H. Xie, J. Li, Y. Xie, J. R. Li, *ACS App.Mater.Interfaces* **2017**, 9, 27027.
- [70] H. Jasuja, N. C. Burtch, Y.-g. Huang, Y. Cai, K. S. Walton, *Langmuir* **2013**, 29, 633.
- [71] A.-A. Al-Terkawi, G. Scholz, F. Emmerling, E. Kemnitz, *Cryst. Growth Des.* **2016**, 16, 1923.
- [72] J. Chun, S. Kang, N. Park, E. J. Park, X. Jin, K.-D. Kim, H. O. Seo, S. M. Lee, H. J. Kim, W. H. Kwon, Y.-K. Park, J. M. Kim, Y. D. Kim, S. U. Son, *J.Am.Chem.Soc.* **2014**, 136, 6786.
- [73] A. M. Cheplakova, K. A. Kovalenko, D. G. Samsonenko, V. A. Lazarenko, V. N. Khrustalev, A. S. Vinogradov, V. M. Karpov, V. E. Platonov, V. P. Fedin, *Dalton Trans.* **2018**, 47, 3283.
- [74] J. G. Nguyen, S. M. Cohen, *J.Am.Chem.Soc.* **2010**, 132, 4560.
- [75] J. Ying, A. Herbst, Y.-X. Xiao, H. Wei, G. Tian, Z. Li, X.-Y. Yang, B.-L. Su, C. Janiak, *Inorg.Chem.* **2018**, 57, 899.
- [76] C. Stastny, B. Dolfus, C. T. Brombach, D. Dresen, S. Disch, R. Glaum, U. Ruschewitz, *Z. Anorg. Allg. Chem.* **2018**, 644, 1423.
- [77] G. Zhang, J. Zhang, P. Su, Z. Xu, W. Li, C. Shen, Q. Meng, *Chem. Commun.* **2017**, 53, 8340.
- [78] N. Ding, H. Li, X. Feng, Q. Wang, S. Wang, L. Ma, J. Zhou, B. Wang, *Journal of the American Chemical Society* **2016**, 138, 10100.
- [79] P. Deria, J. E. Mondloch, E. Tylianakis, P. Ghosh, W. Bury, R. Q. Snurr, J. T. Hupp, O. K. Farha, *J.Am.Chem.Soc.* **2013**, 135, 16801.
- [80] B. Bhattacharya, R. Haldar, D. K. Maity, T. K. Maji, D. Ghoshal, *CrystEngComm* **2015**, 17, 3478.
- [81] G. Huang, Q. Yang, Q. Xu, S.-H. Yu, H.-L. Jiang, *Angewandte Chemie International Edition* **2016**, 55, 7379.
- [82] E. S. Sanil, K.-H. Cho, D.-Y. Hong, J. S. Lee, S.-K. Lee, S. G. Ryu, H. W. Lee, J.-S. Chang, Y. K. Hwang, *Chem. Commun.* **2015**, 51, 8418.

- [83] F. Drache, V. Bon, I. Senkovska, C. Marschelke, A. Synytska, S. Kaskel, *Inorg.Chem.* **2016**, 55, 7206.
- [84] P. Hu, X. Liang, M. Yaseen, X. Sun, Z. Tong, Z. Zhao, Z. Zhao, *Chemical Engineering Journal* **2018**, 332, 608.
- [85] K. Jayaramulu, F. Geyer, M. Petr, R. Zboril, D. Vollmer, R. A. Fischer, *Advanced Materials* **2017**, 29, 1605307.
- [86] K. Tan, N. Nijem, P. Canepa, Q. Gong, J. Li, T. Thonhauser, Y. J. Chabal, *Chem.Mater.* **2012**, 24, 3153.
- [87] J. R. Karra, H. Jasuja, Y.-G. Huang, K. S. Walton, *J.Mater.Chem.A* **2015**, 3, 1624.
- [88] N. u. Qadir, S. A. M. Said, H. M. Bahaidarah, *Micropor. Mesopor. Mat.* **2015**, 201, 61.
- [89] T.-H. Chen, I. Popov, O. Zenasni, O. Daugulis, O. Š. Miljanić, *Chem. Commun.* **2013**, 49, 6846.
- [90] S. Rodríguez-Hermida, M. Y. Tsang, C. Vignatti, K. C. Stylianou, V. Guillerme, J. Pérez-Carvajal, F. Teixidor, C. Viñas, D. Choquesillo-Lazarte, C. Verdugo-Escamilla, I. Peral, J. Juanhuix, A. Verdaguier, I. Imaz, D. MasPOCH, J. Giner Planas, *Angew.Chem.Int.Ed.* **2016**, 55, 16049.
- [91] T.-H. Chen, I. Popov, W. Kaveevivitchai, Y.-C. Chuang, Y.-S. Chen, O. Daugulis, A. J. Jacobson, O. Š. Miljanić, *Nature Commun.* **2014**, 5, 5131.
- [92] T. A. Makal, X. Wang, H.-C. Zhou, *Cryst. Growth Des.* **2013**, 13, 4760.
- [93] D. Ma, Y. Li, Z. Li, *Chem. Commun.* **2011**, 47, 7377.
- [94] S. Mukherjee, A. M. Kansara, D. Saha, R. Gonnade, D. Mullangi, B. Manna, A. V. Desai, S. H. Thorat, P. S. Singh, A. Mukherjee, S. K. Ghosh, *Chem. Eur. J.* **2016**, 22, 10937.
- [95] K. Tan, N. Nijem, Y. Gao, S. Zuluaga, J. Li, T. Thonhauser, Y. J. Chabal, *CrystEngComm* **2015**, 17, 247.
- [96] N. C. Burtch, H. Jasuja, K. S. Walton, *Chem. Rev.* **2014**, 114, 10575.
- [97] Y.-B. Huang, M. Shen, X. Wang, P. Huang, R. Chen, Z.-J. Lin, R. Cao, *J.Catal.* **2016**, 333, 1.
- [98] J. Duan, W. Jin, S. Kitagawa, *Coord.Chem.Rev.* **2017**, 332, 48.
- [99] S. Wang, Z. Kang, B. Xu, L. Fan, G. Li, L. Wen, X. Xin, Z. Xiao, J. Pang, X. Du, D. Sun, *Inorganic Chemistry Communications* **2017**, 82, 64.
- [100] P. G. de Gennes, *Rev. Mod. Phys.* **1985**, 57, 827.
- [101] S. Herminghaus, *EPL* **2007**, 79, 59901.
- [102] D. Quéré *Ann. Rev. Mater. Res.* **2008**, 38, 71.
- [103] D. Bonn, J. Eggers, J. Indekeu, J. Meunier, E. Rolley, *Rev. Mod. Phys.* **2009**, 81, 739.
- [104] H.-J. Butt, K. Graf, M. Kappl, *Physics and Chemistry of Interfaces*, WILEY-VCH, Weinheim, Germany **2003**.
- [105] M. J. Kreder, J. Alvarenga, P. Kim, J. Aizenberg, *Nat. Rev. Mater.* **2016**, 1, 15003.
- [106] I. Shestopalov, J. D. Tice, R. F. Ismagilov, *Lab on a Chip* **2004**, 4, 316.
- [107] Y. Zheng, H. Bai, Z. Huang, X. Tian, F.-Q. Nie, Y. Zhao, J. Zhai, L. Jiang, *Nature* **2010**, 463, 640.
- [108] K.-C. Park, S. S. Chhatre, S. Srinivasan, R. E. Cohen, G. H. McKinley, *Langmuir* **2013**, 29, 13269.
- [109] P. Cheng, X. Quan, S. Gong, X. Liu, L. Yang, in *Advances in Heat Transfer*, Vol. 46 (Eds: Y. I. C. J. P. A. Ephraim M. Sparrow, G. John M), Elsevier **2014**, p. 187.
- [110] K. Rykaczewski, A. T. Paxson, M. Staymates, M. L. Walker, X. Sun, S. Anand, S. Srinivasan, G. H. McKinley, J. Chinn, J. H. J. Scott, K. K. Varanasi, *Scientific Reports* **2014**, 4.

- [111] A. T. Paxson, J. L. Yagüe, K. K. Gleason, K. K. Varanasi, *Adv. Mater.* **2014**, 26, 418.
- [112] C. Yang, U. Kaipa, Q. Z. Mather, X. Wang, V. Nesterov, A. F. Venero, M. A. Omary, *J. Am. Chem. Soc.* **2011**, 133, 18094.
- [113] J. G. Nguyen, S. M. Cohen, *J. Am. Chem. Soc.* **2011**, 132, 4560.
- [114] K. Jayaramulu, K. K. R. Datta, C. Rösler, M. Petr, M. Otyepka, R. Zboril, R. A. Fischer, *Angew. Chem. Int. Ed.* **2016**, 55, 1178.
- [115] Y. Zheng, X. Gao, L. Jiang, *Soft Matter* **2007**, 3, 178.
- [116] Z. Guo, W. Liu, B.-L. Su, *J. Colloid Interface Sci.* **2011**, 353, 335.
- [117] T. Young, *Phil. Trans. R. Soc. Lond.* **1805**, 95, 65.
- [118] K.-Y. Law, *J. Phys. Chem. Lett.* **2014**, 5, 686.
- [119] R. N. Wenzel, *Ind. Eng. Chem.* **1936**, 28, 988.
- [120] A. B. D. Cassie, S. Baxter, *Trans. Faraday Soc.* **1944**, 40, 546.
- [121] A. Lafuma, D. Quéré, *Nat. Mater.* **2003**, 2, 457.
- [122] M. Callies, D. Quéré, *Soft Matter* **2005**, 1, 55.
- [123] H. J. Ensikat, P. Ditsche-Kuru, C. Neinhuis, W. Barthlott, *Beilstein J. Nanotechnol.* **2011**, 2, 152.
- [124] L. Mammen, K. Bley, P. Papadopoulos, F. Schellenberger, N. Encinas, H.-J. Butt, C. K. Weiss, D. Vollmer, *Soft Matter* **2014**, 11, 506.
- [125] M. D'Acunzi, L. Mammen, M. Singh, X. Deng, M. Roth, G. K. Auernhammer, H.-J. Butt, D. Vollmer, *Faraday Discuss.* **2010**, 146, 35.
- [126] L. Feng, S. H. Li, Y. S. Li, H. J. Li, L. J. Zhang, J. Zhai, Y. L. Song, B. Q. Liu, L. Jiang, D. B. Zhu, *Adv. Mater.* **2002**, 14, 1857.
- [127] B. Bhushan, Y. C. Jung, *Prog. Mater. Sci.* **2011**, 56, 1.
- [128] Y. Y. Yan, N. Gao, W. Barthlott, *Adv. Colloid Interface Sci.* **2011**, 169, 80.
- [129] R. H. Dettre, J. Johnson, Rulon E., in *Contact Angle, Wettability, and Adhesion*, DOI: 10.1021/ba-1964-0043.ch008 (Ed: F. M. Fowkes), American Chemical Society, Washington, D.C. **1964**, Ch. 8, p. 136.
- [130] W. Barthlott, C. Neinhuis, *Planta* **1997**, 202, 1.
- [131] X. Gao, L. Jiang, *Nature* **2004**, 432, 36.
- [132] R. Fürstner, W. Barthlott, C. Neinhuis, P. Walzel, *Langmuir* **2005**, 21, 956.
- [133] B. Bhushan, Y. C. Jung, K. Koch, *Langmuir* **2009**, 25, 3240.
- [134] L. Cao, A. K. Jones, V. K. Sikka, J. Wu, D. Gao, *Langmuir* **2009**, 25, 12444.
- [135] S. A. Kulinich, M. Farzaneh, *Appl. Surf. Sci.* **2009**, 255, 8153.
- [136] F. Geyer, M. D'Acunzi, C. Y. Yang, M. Müller, P. Baumli, A. Kaltbeitzel, V. Mailänder, N. Encinas, D. Vollmer, H. J. Butt, *Adv. Mater.* **2018**, 1801324.
- [137] B. J. Privett, J. Youn, S. A. Hong, J. Lee, J. Han, J. H. Shin, M. H. Schoenfish, *Langmuir* **2011**, 27, 9597.
- [138] N. J. Shirtcliffe, G. McHale, M. I. Newton, Y. Zhang, *ACS Appl. Mater. Interfaces* **2009**, 1, 1316.
- [139] R. J. Daniello, N. E. Waterhouse, J. P. Rothstein, *Phys. Fluids* **2009**, 21, 085103.
- [140] F. Geyer, C. Schönecker, H.-J. Butt, D. Vollmer, *Adv. Mater.* **2017**, 29, 1603524.
- [141] M. Paven, P. Papadopoulos, S. Schöttler, X. Deng, V. Mailänder, D. Vollmer, H.-J. Butt, *Nat. Commun.* **2013**, 4, 2512.
- [142] L. Feng, Z. Zhang, Z. Mai, Y. Ma, B. Liu, L. Jiang, D. Zhu, *Angew. Chem. Int. Ed.* **2004**, 43, 2012.
- [143] J. Zhang, S. Seeger, *Adv. Funct. Mater.* **2011**, 21, 4699.
- [144] H. Teisala, M. Tuominen, M. Aromaa, J. M. Mäkelä, M. Stepien, J. J. Saarinen, M. Toivakka, J. Kuusipalo, *Surf. Coat. Technol.* **2010**, 205, 436.

- [145] B. Deng, R. Cai, Y. Yu, H. Q. Jiang, C. L. Wang, J. A. Li, L. F. Li, M. Yu, J. Y. Li, L. D. Xie, Q. Huang, C. H. Fan, *Adv. Mater.* **2010**, 22, 5473
- [146] E. Martines, K. Seunarine, H. Morgan, N. Gadegaard, C. D. W. Wilkinson, M. O. Riehle, *Nano Lett.* **2005**, 5, 2097.
- [147] D. Öner, T. J. McCarthy, *Langmuir* **2000**, 16, 7777.
- [148] B. Qian, Z. Shen, *Langmuir* **2005**, 21, 9007.
- [149] S. Minko, M. Müller, M. Motornov, M. Nitschke, K. Grundke, M. Stamm, *J. Am. Chem. Soc.* **2003**, 125, 3896.
- [150] X. Wang, B. Ding, J. Yu, M. Wang, *Nano Today* **2011**, 6, 510.
- [151] S. Roy, V. M. Suresh, T. K. Maji, *Chem.Sci.* **2016**, 7, 2251.
- [152] K. S. Birdi, CRC Press, Boca Raton **2015**.
- [153] K. S. Birdi, *Handbook of Surface and Colloid Chemistry*, CRC Press, Boca Raton **2015**.
- [154] P. L. du Noüy, *J. Gen. Physiol.* **1925**, 7, 625.
- [155] L. Wilhelmy, *Pogg. Ann.* **1863**, 119, 177.
- [156] W. A. Zisman, in *Contact Angle, Wettability, and Adhesion* (Ed: F. M. Fowkes), American Chemical Society, Washington, D.C. **1964**, Ch. 1, p. 1.
- [157] F. M. Fowkes, *Ind. Eng. Chem.* **1964**, 56, 40.
- [158] D. K. Owens, R. C. Wendt, *J. Appl. Polym. Sci.* **1969**, 13, 1741.
- [159] W. Rabel, *Farbe und Lacke* **1971**, 77, 997.
- [160] D. H. Kaelble, *J. Adhesion* **1970**, 2, 66.
- [161] N. L. Jarvis, W. A. Zisman, *Surface Chemistry of Fluorochemicals*, U.S. Naval Research Laboratory, Washington, D.C. **1965**.
- [162] J. J. Gilman, *J. Appl. Phys.* **1960**, 31, 2208.
- [163] T. Nishino, M. Meguro, K. Nakamae, M. Matsushita, Y. Ueda, *Langmuir* **1999**, 15, 4321.
- [164] S. Mohammadi-Jam, K. E. Waters, *Adv. Colloid Interface Sci.* **2014**, 212, 21.
- [165] R. Ho, J. Y. Y. Heng, *KONA Powder Part. J.* **2013**, 30, 164.
- [166] J. Schultz, L. Lavielle, C. Martin, *J. Adhesion* **1987**, 23, 45.
- [167] G. M. Dorris, D. G. Gray, *J. Colloid Interface Sci.* **1980**, 77, 353.
- [168] S. C. Das, I. Larson, D. A. V. Morton, P. J. Stewart, *Langmuir* **2011**, 27, 521.
- [169] C. Della Volpe, S. Siboni, *J. Colloid Interface Sci.* **1997**, 195, 121.
- [170] L. Lapčík, M. Otyepkaa, E. Otyepková, B. Lapčíková, R. Gabriel, A. Gavenda, B. Prudilová, *Curr. Opin. Colloid In.* **2016**, 24, 64.
- [171] P. Lazar, E. Otyepková, P. Banáš, A. Fargašová, K. Šafařová, L. Lapčík, J. Pechoušek, R. Zbořil, M. Otyepka, *Carbon* **2014**, 73, 448.
- [172] A. Ferguson, A. Harvey, I. J. Godwin, S. D. Bergin, J. N. Coleman, *2D Mater.* **2017**, 4, 015040.
- [173] E. Otyepkova, P. Lazar, J. Luxa, K. Berka, K. Cepe, Z. Sofer, M. Pumera, M. Otyepka, *Nanoscale* **2017**, 9, 19236.
- [174] T. Huhtamäki, X. Tian, J. T. Korhonen, R. H. A. Ras, *Nat. Protoc.* **2018**, 13, 1521.
- [175] X. Zhang, F. Shi, J. Niu, Y. Jiang, Z. Wang, *J. Mater. Chem.* **2008**, 18, 621.
- [176] F. Schellenberger, N. Encinas, D. Vollmer, H.-J. Butt, *Phys. Rev. Lett.* **2016**, 116, 096101
- [177] P. Papadopoulos, L. Mammen, X. Deng, D. Vollmer, H.-J. Butt, *Proc. Natl. Acad. Sci. U. S. A.* **2013**, 110, 3254.
- [178] L. Gao, T. J. McCarthy, *Langmuir* **2006**, 22, 6234.
- [179] H.-J. Butt, R. Berger, W. Steffen, D. Vollmer, S. A. L. Weber, *Langmuir* **2018**, 34, 11292.

Hydrophobic Metal–Organic Frameworks, F. Geyer et. al. ,*Adv. Mater.* 2019, 1900820, DOI: 10.1002/adma.201900820

- [180] R. H. A. Ras, X. Tian, I. S. Bayer, in *Handbook of Nanocellulose and Cellulose Nanocomposites*, Vol. 1 (Eds: H. Kargarzadeh, I. Ahmad, S. Thomas, A. Dufresne), Wiley - VCH, Weinheim, Germany **2017**, Ch. 22.
- [181] C. J. Long, J. F. Schumacher, A. B. Brennan, *Langmuir* **2009**, 25, 12982.
- [182] M. Miwa, A. Nakajima, A. Fujishima, K. Hashimoto, T. Watanabe, *Langmuir* **2000**, 16, 5754.
- [183] A. Marmur, *Langmuir* **2004**, 20, 3517.
- [184] N. Gao, F. Geyer, D. W. Pilat, S. Wooh, D. Vollmer, H.-J. Butt, R. Berger, *Nat. Phys.* **2018**, 14, 191.
- [185] L. Gao, T. J. McCarthy, *J. Am. Chem. Soc.* **2006**, 128, 9052.
- [186] F. Schellenberger, J. Xie, N. Encinas, A. Hardy, M. Klapper, P. Papadopoulos, H.-J. Butt, D. Vollmer, *Soft Matter* **2015**, 11, 7617.
- [187] T.-S. Wong, S. H. Kang, S. K. Y. Tang, E. J. Smythe, B. D. Hatton, A. Grinthal, J. Aizenberg, *Nature* **2011**, 477, 443.
- [188] L. Wang, T. J. McCarthy, *Angew. Chem. Int. Ed.* **2016**, 55, 244.
- [189] Y. I. Frenkel, *Journal of Experimental and Theoretical Physics* **1948**, 18, 658.
- [190] K. Kawasaki, *J. Colloid Sci.* **1960**, 15, 402.
- [191] R. A. Brown, F. M. Orr Jr., L. E. Scriven, *J. Colloid Interface Sci.* **1980**, 73, 76.
- [192] C. W. Extrand, A. N. Gent, *J. Colloid Interface Sci.* **1990**, 138, 431.
- [193] C. W. Extrand, Y. Kumagai, *J. Colloid Interface Sci.* **1995**, 170, 515.
- [194] M. Eddaoudi, J. Kim, N. Rosi, D. Vodak, J. Wachter, M. Keefe, O. M. Yaghi, *Science* **2002**, 295, 469.
- [195] A. Schneemann, V. Bon, I. Schwedler, I. Senkovska, S. Kaskel, R. A. Fischer, *Chem.Soc.Rev.* **2014**, 43, 6062.
- [196] Z. Wang, S. M. Cohen, *Chem.Soc.Rev.* **2009**, 38, 1315.
- [197] M. Zhang, X. Xin, Z. Xiao, R. Wang, L. Zhang, D. Sun, *J.Mater.Chem.A* **2017**, 5, 1168.
- [198] K. P. Rao, M. Higuchi, J. Suryachandram, S. Kitagawa, *J.Am.Chem.Soc.* **2018**, 140, 13786.
- [199] V. Georgakilas, M. Otyepka, A. B. Bourlinos, V. Chandra, N. Kim, K. C. Kemp, P. Hobza, R. Zboril, K. S. Kim, *Chemical Reviews* **2012**, 112, 6156.
- [200] A. Bakandritsos, M. Pykal, P. Błoński, P. Jakubec, D. D. Chronopoulos, K. Poláková, V. Georgakilas, K. Čépe, O. Tomanec, V. Ranc, A. B. Bourlinos, R. Zbořil, M. Otyepka, *ACS Nano* **2017**, 11, 2982.
- [201] K. Jayaramulu, F. Geyer, M. Petr, R. Zboril, D. Vollmer, R. A. Fischer, *Adv.Mater.* **2017**, 29.
- [202] S. Roy, V. M. Suresh, A. Hazra, A. Bandyopadhyay, S. Laha, S. K. Pati, T. K. Maji, *Inorg.Chem.* **2018**, 57, 8693.
- [203] P. Aussillous, D. Quéré, *Nature* **2001**, 411, 924.
- [204] G. McHale, M. I. Newton, *Soft Matter* **2011**, 7, 5473.
- [205] S. Fujii, S. Yusa, Y. Nakamura, *Adv. Funct. Mater.* **2016**, 26, 7206.
- [206] W. Fan, X. Liu, X. Wang, Y. Li, C. Xing, Y. Wang, W. Guo, L. Zhang, D. Sun, *Inorganic Chemistry Frontiers* **2018**, 5, 2445.
- [207] R. K. Gupta, G. J. Dunderdale, M. W. England, A. Hozumi, *J.Mater.Chem.A* **2017**, 5, 16025.
- [208] X. Zhang, Y. Zhao, S. Mu, C. Jiang, M. Song, Q. Fang, M. Xue, S. Qiu, B. Chen, *ACS App.Mater.Interfaces* **2018**, 10, 17301.
- [209] R. Breslow, *Acc.Chem.Res.* **1991**, 24, 159.

Hydrophobic Metal–Organic Frameworks, F. Geyer et. al. ,*Adv. Mater.* 2019, 1900820, DOI: 10.1002/adma.201900820

- [210] L. Luza, A. Gual, C. P. Rambor, D. Eberhardt, S. R. Teixeira, F. Bernardi, D. L. Baptista, J. Dupont, *Phys.Chem.Chem.Phys.* **2014**, *16*, 18088.
- [211] K. Yuan, T. Song, D. Wang, X. Zhang, X. Gao, Y. Zou, H. Dong, Z. Tang, W. Hu, *Angew. Chem. Int. Ed.* **2018**, *57*, 5708.
- [212] L. Li, Q. Yang, S. Chen, X. Hou, B. Liu, J. Lu, H.-L. Jiang, *Chem. Commun.* **2017**, *53*, 10026.

TOC

This review critically summarizes recent progress in the categories, synthetic routes, properties, critical challenges of characterization and applications of hydrophobic metal-organic frameworks.

